



저작자표시-비영리-변경금지 2.0 대한민국

이용자는 아래의 조건을 따르는 경우에 한하여 자유롭게

- 이 저작물을 복제, 배포, 전송, 전시, 공연 및 방송할 수 있습니다.

다음과 같은 조건을 따라야 합니다:



저작자표시. 귀하는 원저작자를 표시하여야 합니다.



비영리. 귀하는 이 저작물을 영리 목적으로 이용할 수 없습니다.



변경금지. 귀하는 이 저작물을 개작, 변형 또는 가공할 수 없습니다.

- 귀하는, 이 저작물의 재이용이나 배포의 경우, 이 저작물에 적용된 이용허락조건을 명확하게 나타내어야 합니다.
- 저작권자로부터 별도의 허가를 받으면 이러한 조건들은 적용되지 않습니다.

저작권법에 따른 이용자의 권리는 위의 내용에 의하여 영향을 받지 않습니다.

이것은 [이용허락규약\(Legal Code\)](#)을 이해하기 쉽게 요약한 것입니다.

[Disclaimer](#)

Prediction of immune checkpoint inhibitor
response based on
immune phenotype classification

Eunyoung Kim

Department of Medical Science

The Graduate School, Yonsei University

Prediction of immune checkpoint inhibitor
response based on
immune phenotype classification

Directed by Professor Sangwoo Kim

The Doctoral Dissertation
submitted to the Department of Medical Science,
the Graduate School of Yonsei University
in partial fulfillment of the requirements for the degree of
Doctor of Philosophy in Medical Science

Eunyoung Kim

December 2023

This certifies that the Doctoral Dissertation
of Eunyoung Kim is approved.

Thesis Supervisor : Sangwoo Kim

Thesis Committee Member#1 : Jae-Ho Cheong

Thesis Committee Member#2 : Soonmyung Paik

Thesis Committee Member#3 : June-Yong Lee

Thesis Committee Member#4 : Tae Hyun Hwang

The Graduate School
Yonsei University

December 2023

ACKNOWLEDGEMENTS

학위과정을 진행하는 동안 많은 분들의 도움으로 여기까지 올 수 있었습니다. 이 자리를 빌려 도움 주신 모든 분께 깊은 감사의 인사를 전합니다. 가장 먼저, 김상우 교수님께 진심으로 감사드립니다. 교수님의 변함 없는 믿음과 지혜로운 조언과 지도 덕분에 한 명의 연구자로서 성장할 수 있었습니다.

학위논문 심사를 맡아 주시고, 소중한 고견 나누어 주신 교수님들께도 감사의 인사를 전합니다. 연구자의 마음가짐과 생각의 틀을 넓혀 주신 정재호 교수님, 언제나 활발한 토론으로 방향성을 제시하여 주신 백순명 교수님, 따뜻한 조언으로 정교함을 높여 주신 이준용 교수님, 반대의 시차에 개의치 않고 함께 고민해 주신 황태현 교수님께 각별한 감사의 말씀을 전합니다. 교수님들께 받은 영감과 도움으로 이제 저는 연구자로서 세상에 나아가려 합니다. 내려주신 가르침을 토대로 언제나 올바른 연구자에 대해 고민하고 노력하겠습니다.

대학원은 저에게 있어 새로운 도전이자, 지식을 쌓고 열정을 다했던 귀중한 시간이었습니다. 열정을 쏟아부은 결과물들이 발행되는 기쁨과 일부는 손 틈 사이로 흘러내리는 모래 같은 아쉬움까지 경험하며 다채로운 시간을 보냈습니다.

학위를 마무리하는 이 순간 되돌아보니, 참 많은 것을 얻었다고 느낍니다. 같은 길을 걸으며 함께하는 소중한 인연들이 생겼고, TGIL의 훌륭한 선후배님들의 밝고 긍정적인 모습에 많은 힘을 얻었습니다. 그리고 어려움을 함께 극복해 나간 우리 면역팀, 함께한 시간 동안 많은 것을 배웠기에 미안함과 감사의 인사를 전합니다. 무엇보다 끝까지 포기하지 않고 완주한 저 자신에게 고맙고 대견하다고 말해주고 싶습니다. 우리 아빠, 엄마, 내 동생 지영이, 가족들의 묵묵한 지지와 응원 속에 학위과정을 마무리할 수 있어 다행이고 감사드립니다. 마지막으로, 언제나 믿어주고 나의 든든한 버팀목이 되어준 그 사람에게 함께 해주어서 고맙다는 말을 전합니다.

TGIL에서의 소중한 추억들을 원동력으로 삼아 새로운 세상으로 힘차게 한 걸음 나아가 보려 합니다. 이제 미래에 대한 설렘을 안고 새로운 여정을 시작합니다.

TABLE OF CONTENTS

ABSTRACT	vii
I. INTRODUCTION	1
1. History of cancer immunotherapy.....	1
2. Comprehension of the immune microenvironment.....	2
3. Relation between the TME and ICI response	4
4. Importance of immune phenotype	6
5. The tumor-immunity cycle and immune phenotype	8
6. Prediction of ICI response based on immune phenotype.....	1 1
II. MATERIALS AND METHODS.....	1 3
1. Data acquisition.....	1 3
2. Quantification of gene expression from bulk RNA sequencing	1 7
3. Estimation of immune phenotype specific ICI response.....	1 7
4. Collection of immune phenotype specific features	1 8
A. Prevalence of immune cell type	1 8
B. The fraction of stromal and immune cells.....	1 9
C. Immune phenotype related gene.....	1 9
5. Classification model of immune phenotype.....	2 0

6. Generation of TIDE and IMPRES score.....	2 0
7. Gene set enrichment analysis.....	2 1
8. Statistical analysis	2 1
III. RESULTS.....	2 2
1. Expression of <i>PD-1</i> and <i>PD-L1</i> in relation to immune phenotype and ICI response	2 2
2. Overview of CLIPS.....	2 4
A. Classification of immune phenotype.....	2 5
B. Prediction of immune phenotype-specific ICI response	2 7
3. Expression of <i>PD-1</i> and <i>PD-L1</i> in predicted immune phenotypes	3 1
4. Overall survival.....	3 3
5. Evaluation of CLIPS for ICI response prediction.....	3 4
A. Performance evaluation in test dataset	3 4
C. Performance evaluation in independent validation dataset within cancer types.....	4 1
6. Genomic characteristics of ICI response based on immune phenotype	4 4
IV. DISCUSSION.....	4 8
V. CONCLUSION.....	5 5

REFERENCES.....	5 8
APPENDICES	6 5
ABSTRACT(IN KOREAN).....	6 6
PUBLICATION LIST.....	6 9

LIST OF FIGURES

Figure 1. The tumor-immunity cycle and immune phenotypes.	9
Figure 2. The association between the immune phenotype and ICI response.....	2 3
Figure 3. Overview of CLIPS.....	2 4
Figure 4. Selected features for immune phenotype classification. 2	6
Figure 5. Performance of five immune phenotype multi-class classification.	2 6
Figure 6. Prediction of immune phenotype-specific ICI response based on DEGs.....	2 7
Figure 7. Heatmap of DEGs from immune phenotype-specific ICI response groups.....	2 8
Figure 8. The ratio of total rank within ICI response.	3 0
Figure 9. Comparison of ICI response DEGs according to cancer types.	3 0
Figure 10. The association between the ICI response and predicted immune phenotype from CLIPS.....	3 2
Figure 11. Overall survival analysis according to ICI response and immune phenotypes.....	3 3
Figure 12. Comparison of the performance of five ICI response prediction tools with MCC and Accuracy in test dataset.	3 4

Figure 13. Comparison of the performance of five ICI response prediction tools with all performance measures in test dataset. 3 5

Figure 14. MCC and Accuracy within independent validation dataset according to anti-PD-1 treatment types. 4 0

Figure 15. Performance evaluation for independent validation dataset according to anti-PD1 treatment types. 4 0

Figure 16. MCC and Accuracy within independent validation dataset according to cancer types..... 4 3

Figure 17. Performance evaluation for independent validation dataset according to cancer types..... 4 3

Figure 18. GSEA with hallmark gene-set for immune phenotype-specific ICI response..... 4 7

LIST OF TABLES

Table 1. Cohort information of the study	1 5
Table 2. Data for immune phenotype classification	1 6
Table 3. Data for immune phenotype-specific ICI response prediction	1 6
Table 4. Confusion matrix of test dataset within immune phenotype	3 7
Table 5. Performance indicator in immune phenotypes from IHC	3 7
Table 6. Confusion matrix of independent validation with combination treatment	5 4

ABSTRACT

**Prediction of immune checkpoint inhibitor response
based on immune phenotype classification**

Eunyoung Kim

*Department of Medical Science
The Graduate School, Yonsei University*

(Directed by Professor Sangwoo Kim)

The immune phenotype reflects the immune response and is associated with biological mechanisms that can interfere with the elimination of cancer. Additionally, the immune phenotype is known to influence the overall survival of melanoma patients receiving immune checkpoint inhibitor (ICI) treatment. In order to improve the effectiveness of personalized immune therapy, it is essential to develop an algorithm that can accurately and objectively predict an individual's immune environment based on gene expression data from bulk RNA sequencing.

The study aims to develop an algorithm called CLIPS (CLassification of Immune Phenotypes-Specific ICI response) using gene expression data from bulk RNA sequencing. The CLIPS predict an individual's immune phenotype and their ICI response based on immune phenotype. The CLIPS demonstrates a robust prediction performance with an AUC of 0.76, enabling the accurate prediction of patient-specific immune phenotypes, thereby replacing the conventional immunohistochemistry (IHC) technique. The accuracy of the previously published predictive tools for ICI treatment response, TIDE and IMPRES, were compared with CLIPS using independent validation data from

41 melanoma patients. The results showed that TIDE achieved an accuracy of 0.63, IMPRES attained an accuracy of 0.58, while CLIPS achieved a higher accuracy of 0.76 based on predicted immune phenotypes, leading to more accurate predictions of individual patient's responses to ICI. In addition, CLIPS can predict responsiveness with high accuracy, regardless of cancer type or type of ICI treatment.

Furthermore, this study revealed the association between immune phenotype and the expression of *PD-1* and *PD-L1* genes as well as the ICI response. The expression of *PD-1* and *PD-L1* genes was significantly higher in the inflamed immune phenotype compared to the excluded and desert immune phenotypes. Also, the common upregulation of E2F target related genes in both the excluded and desert immune phenotypes in the ICI response group was observed. The E2F pathway appears to increase the expression of *PD-1*, thereby enhancing susceptibility to ICI. Likewise, the IL-6/JAK/STAT3 signaling pathway was predominantly present in the inflamed immune phenotype, suggesting a favorable response to ICI due to increased *PD-L1* gene expression mediated by IL-6 secretion.

This study provides important insights into the classification of immune phenotypes, facilitating the development of personalized treatment strategies. Understanding the immune phenotype not only aids in the comprehension of functional characteristics of the immune system but also expands the identification of additional subtypes that can be utilized to predict ICI response.

In conclusion, this research contributes significantly to providing personalized treatment options based on understanding and predicting immune phenotypes. This approach has the potential to enhance cancer patient survival rates and optimize the efficacy of immunotherapies.

Key words : immune phenotype, immune checkpoint inhibitor, immune profiling, immunotherapy, tumor microenvironment, immunoinformatics, next-generation sequencing

Prediction of immune checkpoint inhibitor response based on immune phenotype classification

Eunyoung Kim

*Department of Medical Science
The Graduate School, Yonsei University*

(Directed by Professor Sangwoo Kim)

I. INTRODUCTION

1. History of cancer immunotherapy

In the early stages of cancer immunotherapy, non-specific therapies were commonly used to boost the immune system's response to cancer. These therapies aimed to enhance the overall immune response against cancer cells. Prominent among these non-specific therapies were the Bacillus Calmette-Guérin (BCG) vaccine, int, and interleukin-2 (*IL-2*) cytokine. As the field of immunotherapy advanced, there was a shift towards more personalized and targeted approaches. Patient-derived cancer vaccines and immune checkpoint inhibitors (ICI) are examples of these personalized approaches¹. The patient-derived cancer vaccines are designed to target specific neoantigens found on a patient's tumor cells, which are unique to the patient and not present in healthy cells². These vaccines stimulate an immune response against the tumor cells, allowing for a targeted and potentially more effective immune response against the specific cancer. The ICI treatment, such as programmed cell death protein

1 (*PD-1*) inhibitors, and programmed death-ligand 1 (*PD-L1*) inhibitors, are a type of therapy that work by blocking checkpoint proteins in the immune system. The mechanism of action of anti-*PD-1* and anti-*PD-L1* therapy involves blocking the interaction of *PD-1* and *PD-L1*, which in turn abolishes the inhibition of CD8+ T cells, thereby enhancing the antitumor immune response. This mechanism helps in restoring the activity of T cells to recognize and target cancer cells.

The ICI treatment has been reported to improve survival period in diverse cancer types, including non-small cell lung cancer and metastatic melanoma³. This improvement, however, does not present uniformly among all patients. Observations of treatment responses reveal a significant heterogeneity among individuals. For a substantial subset of patients receiving ICI therapies, the clinical benefit remains unfortunately limited. This suggests that while ICIs have revolutionized cancer treatment with marked success in certain cases, they are not universally effective. For the majority of patients undergoing ICI treatment, the derived benefit is notably minimal. This underlines the necessity for continued research to understand and overcome the mechanisms of resistance and to identify biomarkers capable of predicting response to ICI therapy.

2. Comprehension of the immune microenvironment

The Cancer Genome Atlas (TCGA) has contributed significantly to understanding the genomic landscape of many types of cancers, which has been critical in designing targeted immunotherapies. Both of these therapeutic advancements happened concurrently and have synergistically advanced the field of oncology. Nonetheless, our understanding of the biology of the immune microenvironment, a critical determinant of the effectiveness of such therapies, remains incomplete. The immune microenvironment, comprising various immune cells in and around the tumor, plays a pivotal role in

modulating the body's immune response against cancer cells. Therefore, it plays a significant role in determining the success of immunotherapies. Understanding this intricate microenvironment is key to designing more effective immunotherapy strategies and predicting which patients will respond best to these therapies. Continued research in this area is necessary further to optimize treatment plans and outcomes for cancer patients. The large-scale study conducted a comprehensive analysis of the immune tumor microenvironment (TME) in 33 different types of cancer using various immunogenomic methods⁴. Some of these methods included the assessment of total lymphocytic infiltrate, immune cell fractions from deconvolution analysis of mRNA sequencing data, immune gene expression signatures, neoantigen prediction, TCR and BCR repertoire inference, and changes in somatic DNA. The integration of these methods allowed for a thorough characterization of the TME across multiple cancer types as part of the TCGA project. Through this approach, the large-scale study discovered and detailed six immune subtypes present across various tumor types. These findings could potentially contribute to therapeutic strategies and have implications for predicting disease progression, ultimately enhancing cancer management. A comparison was made regarding the immune content present in various immune and cancer subtypes. Additionally, somatic alterations that correlated with changes in the TME were identified. The identification of six consistent and reproducible immune subtypes that cover nearly all human cancers has been made. These immune subtypes correlated with prognosis and displayed genetic and immune modulatory changes that could mold the unique immune environments observed. As the discovery of the significant impact of the tumor immune microenvironment on prognosis and treatment efficacy deepens, identifying the immune subtype of a tumor may become a critical factor in predicting the outcome of the disease. This approach has the potential to offer more reliability compared to only relying on the unique features of each cancer types.

3. Relation between the TME and ICI response

Features of the tumor included cancer genomes and microenvironment is recognized as the main factors that response and resistance to ICI. Somatic mutations resulting from mutations at the genomic level, such as DNA mismatch repair genes, oncogenes and tumor suppressor genes, are considered biomarkers to predict the therapeutic effects of ICI⁵. A recent study has amplified our understanding of the intricate orchestration of the immune response within the TME of mismatch repair-deficient tumors. Deficiency in the DNA mismatch repair system leads to a state of microsatellite instability, resulting in high rates of genetic mutations. This heightened mutational profile can render the tumor more immunogenic, thereby eliciting a conspicuous immune reaction. The study demonstrated that numerous immune checkpoint ligands, including *PD-1*, *PD-L1*, cytotoxic T-lymphocyte-associated protein 4 (*CTLA-4*), lymphocyte-activation gene 3 (*LAG-3*), and indoleamine 2,3-dioxygenase (*IDO*), were strongly expressed in the mismatch repair-deficient TME. These markers play a crucial role in modulating the immune response, often serving as mechanisms for cancer cells to impede immune activity and evade destruction. The high mutation burden has proven to be more effective in the treatment of ICI than patients with low mutation burden⁶. This correlation further supports the notion that mutation-associated neoantigen recognition plays a significant role in driving the endogenous antitumor immune response. The observed findings suggest that the immune infiltrate associated with mismatch repair-deficient carcinomas is associated with neoantigens. Neoantigens are altered protein sequences derived from somatic mutations in the tumor genome, and they are recognized by the immune system as foreign or abnormal. The presence of a heightened immune response within these tumors, therefore, implies that the immune system is actively targeting and responding to neoantigens generated as a consequence of the genomic

instability associated with DNA mismatch repair deficiency. Previous studies have shown that mismatch repair-deficient carcinomas are associated with an immune infiltrate dominated by CD8⁺ T cells, increased levels of tumor-infiltrating lymphocytes (TILs), and upregulation of immune checkpoint molecules such as *PD-1* and *PD-L1*⁷. These findings suggest that these tumors may be more responsive to anti-PD-1 and anti-PD-L1 immunotherapy.

Although TILs such as CD8⁺ T cells is a potential predictive biomarker for patient's prognosis also carcinogenesis pathways influence the TME⁸. The ability to exclude invasive immune cells from the TME may change the response to immune checkpoint inhibitors by assisting or hindering the anti-tumor immune response⁹. Moreover, the spatial distribution of immune cells within the TME, known as immune cell topography, has become a significant prognostic factor and indicator of therapeutic response in solid tumors¹⁰. The TME, conceptualized as the cellular environment in which the tumor exists, is a complex network comprised of various cell types including not only the malignant cells themselves but also blood vessels, antigen-presenting cells (APCs), myeloid-derived suppressor cells (MDSCs), tumor-associated macrophages (TAMs), fibroblasts, and indeed, the aforesaid TILs. The aforementioned elements are not solely present within the TME, but rather engage in a reciprocal interaction that influences the immune response to tumors¹¹.

Nevertheless, the complex network within the TME is not randomly distributed; instead, they follow distinct patterns, giving rise to what is commonly referred to as the immune cell topography. This spatial distribution of immune cells within the TME has emerged as a significant prognostic factor and plays a key role in indicating the therapeutic response in solid tumors. This distribution has predictive significance in terms of prognosis, TME, and immunotherapy for patients with esophageal cancer and colorectal cancer¹². Overall, The immune cell topography within the TME plays a crucial role in predicting therapeutic

response in solid tumors¹³. These cells reflect the balance of effector and suppressive activity within the TME, thus influencing the clinical response to treatment.

The acquisition of comprehensive understanding regarding the TME across different subtypes of tumors is of utmost importance in the development of precise therapeutic approaches. This significance arises from the diverse nature of the TME, its involvement in the modulation of immune responses, its contribution to the development of drug resistance, its potential for the identification of biomarkers, and the exploration of novel therapeutic targets. The acquisition of this augmented knowledge has the potential to incite an immune reaction and enhance treatment efficacy in individuals afflicted with solid tumors. This is achieved through the modulation of the clinical response to treatment, the initiation of an immune response, the optimization of immunotherapeutic approaches, the surmounting of immune suppression, the customization of treatments, the mitigation of adverse effects, the prognostication of therapeutic response, and the provision of insights for combination therapies.

4. Importance of immune phenotype

Indeed, the infiltration of T cells in the TME plays an essential part in determining the effectiveness of ICI treatment, a powerful class of immunotherapeutic agents. To further clarify, the TME is often classified into two distinct states known as cold tumors and hot tumors for a better understanding of the immune response¹⁴. The hot tumors are characterized by a TME that is abundant in TILs, overexpression of *PD-L1* and preexisting antitumor immune responses. On the other hand, cold tumors have the opposite characteristics, with a lack of TILs and lower levels of immune activity. In the case of cold tumors, the effectiveness of ICI diminishes significantly, predominantly due to the absence of T-cell infiltration. This obstacle not only

hampers overcoming these tumors but also restricts the full exploitation of the benefits immunotherapy can offer. To effectively overcome this hurdle and maximize the advantages of immunotherapy, it is important to acquire a comprehensive understanding of the factors that promote the infiltration of T-cells into tumors. A promising area of research in the field of immunotherapy is the conversion of cold tumors into hot tumors, identified by an enhanced T-cell presence and activity. Triumphantly actualizing this transition has potential to boost the efficacy of ICIs significantly. Additionally, this progression points towards a promising enhancement in the successful treatment of patients battling malignant tumors, offering a hopeful prospect in this area of study.

The more comprehensive classification is based on the spatial distribution of TILs, known as immune phenotype, which comprises immune-inflamed, immune-excluded and immune-desert phenotypes¹⁵. This classification expands upon the previous division into cold and hot tumors. The immune phenotypes provide a subjective framework to profile the immune contexture in solid tumors e inflamed defines states in which sufficient immune cells with active immune response¹⁶. The immune-inflamed phenotype is characterized by the infiltration of CD8⁺ T cells into the tumor epithelium. In these cases, the immune cells penetrate the tumor tissue and can potentially target and eliminate cancer cells On the other hand, the immune-excluded phenotype is typified by a particular pattern where CD8⁺ T cells, instead of infiltrating the tumor epithelium, accumulate with greater prevalence in the tumor stroma. Implying that while immune cells are indeed present, a barrier to effective interaction exists. Consequently, they cannot engage with the tumor cells directly and exert their critical antitumor activity. Conversely, the immune-desert phenotype is characterized by the absence or minimal presence of CD8⁺ T cells within the tumor. This insufficient immune cell infiltration hampers the immune response against the tumor, potentially allowing it to evade detection

and destruction.

The immune-desert phenotype and the immune-excluded phenotype can both be considered as non-inflamed tumors, commonly known as cold tumors¹². These tumor types share similarities in terms of lacking effective immune response within the TME. The immune-inflamed phenotype pertains to a specific type of tumors that are distinguished by significant immune cell presence and a prevailing pro-inflammatory condition. These tumors, commonly referred to as hot tumors, are defined by the conspicuous accumulation of immune cells and a heightened state of inflammation within TME.

5. The tumor-immunity cycle and immune phenotype

The description of the tumor-immunity cycle provides a comprehensive framework for understanding the dynamic interaction between the immune system, particularly CD8⁺ T lymphocytes, and tumor cells¹⁷. The tumor-immunity cycle consists of a sequence of seven steps that are essential for mounting an effective anti-tumor immune response (**Figure 1**). These seven steps include: 1) tumor antigen release: the initial step involves the release of tumor-specific antigens into the TME. 2) tumor antigen processing and presentation: antigen-presenting cells capture the released antigens and present them to T cells. 3) priming and activation of T cells: tumor antigen presentation leads to the priming and activation of CD8⁺ T cells. These activated T cells are specific for the tumor antigens and are poised to attack tumor cells. 4) trafficking of T cells to tumors: activated T cells travel through the bloodstream, seeking out the tumor site. 5) infiltration of T cell into tumors: In this step, T cells must successfully infiltrate the tumor site, entering the tumor parenchyma from the vasculature or tumor periphery. 6) recognition of cancer cells: T cells recognize and bind to cancer cells that display the specific antigens they are primed against. 7) killing of cancer cells: T cells exert cytotoxic effects on

cancer cells through the release of cytotoxic molecules or through interaction with death receptors on cancer cells.

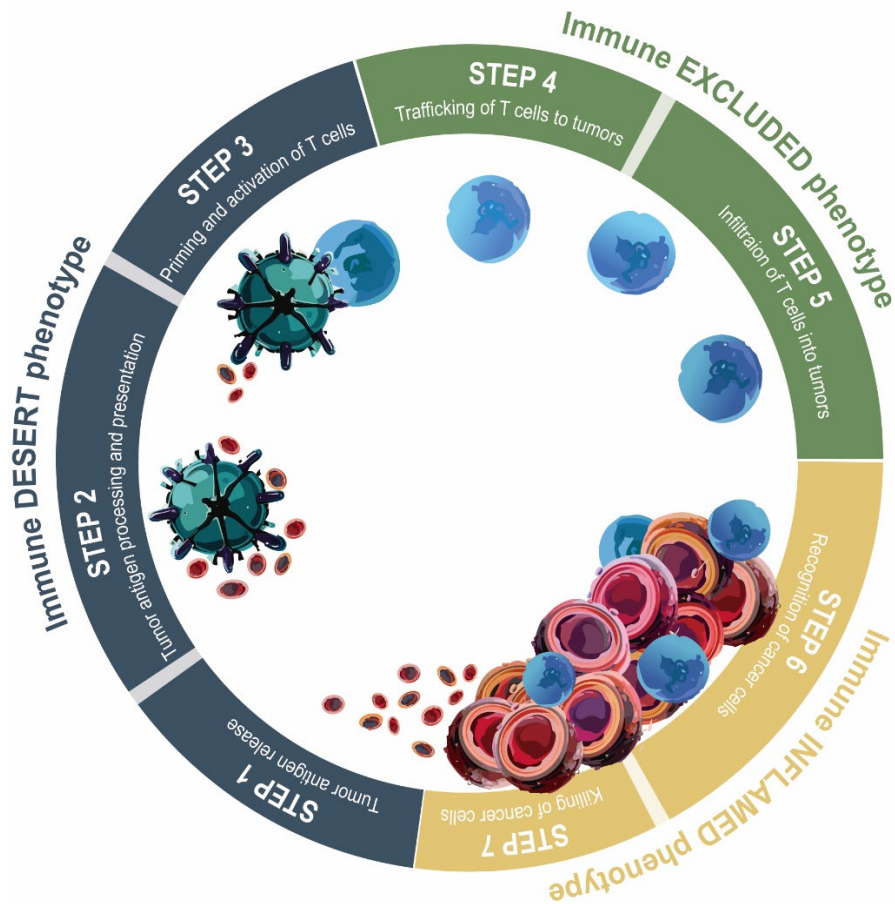


Figure 1. The tumor-immunity cycle and immune phenotypes.

The tumor-immunity cycle consists of seven steps. Step 1-3 are associated with desert immune phenotype (blue), step 4 and 5 are related with excluded immune phenotype (green), and the last two steps are linked to the immune inflamed immune phenotype (yellow).

Importantly, the tumor-immunity cycle is a dynamic and self-perpetuating process. This continuous cycle is indispensable for maintaining a potent and consistent immune response against the tumor. The concept of immune

phenotypes, as described in the context of the immune-desert, immune-excluded, and immune-inflamed phenotypes, reflects the diverse ways in which this cycle can be disrupted or impeded in the context of different tumors. Among the 7 steps of the tumor-immunity cycle, problems occur in the initial three stages which include the tumor antigen release, tumor antigen processing and presentation, as well as priming and activation of T cells. These challenges ultimately lead to the emergence of the immune-desert phenotype, characterized by the absence of immune cells in nearby of the tumor. In the event of complications in the 4 and 5 steps of trafficking of T cells to tumors and infiltration of T cell into tumors, the immune-excluded phenotype occurs where immune cells cannot approach the tumor. When challenges arise during steps 6 and 7 of the tumor-immunity cycle, which involve the recognition of cancer cells and killing of cancer cells, the situation can be grouped as an immune-inflamed phenotype. The issue arises in scenarios with the presence of a sufficient amount of immune cells in the area of the tumor, but the challenges continue due to the presence of T-cell exhaustion or activation of checkpoint mechanisms. Hence, it is imperative to comprehend the complex processes of the tumor-immunity cycle, encompassing potential perturbations that result from diverse immune phenotypes. This understanding is key to devising targeted therapeutic strategies, such as immunotherapies.

The clinical responses to anti-PD-1 and anti-PD-L1 therapy are commonly observed in patients with an immune-inflamed phenotype. The overexpression of PD-L1 on tumor cells or TILs can induce T cell exhaustion, thus attenuated tumor-specific immunity accelerating tumor progression¹⁸. The immune-inflamed phenotype indicates a possible existence of an initial anti-cancer immune response, which was likely hindered due to immunosuppression in the tumor bed. The immune-inflamed phenotype is generally associated with higher response rates to anti-PD-1 and anti-PD-L1 therapy.

6. Prediction of ICI response based on immune phenotype

Likewise, PD-1 inhibitors and PD-L1 inhibitors work by blocking the negative regulatory signal pathways and allowing T cells to be released from an exhausted state. When patients are treated with anti-PD-1 and anti-PD-L1 therapy, T cells associated with the stroma may show signs of activation and proliferation, but they do not effectively infiltrate the tumor. As a result, it is generally uncommon to observe clinical responses in immune-excluded phenotypes. These characteristics suggest that there might have been a pre-existing anti-tumor response, however, it was made ineffectual due to an obstruction blocking tumor infiltration through the stroma, or due to the containment of immune cells within the stroma.

The progression of T-cell migration through the tumor stroma is thus the pivotal phase in the cancer-immunity cycle for the immune-desert phenotype. The main characteristic of the immune-desert phenotype is the presence of a non-inflamed TME with few or no CD8-carrying T cells. As expected, the tumors with immune-desert phenotype rarely respond to anti-PD-1 and anti-PD-L1 therapy. This phenotype probably reflects the absence of pre-existing anti-tumor immunity, which suggests that the generation of tumor-specific T cells is the limiting factor in this process.

Predicting the response to ICI based on immune phenotypes is an important area of study in immunotherapy research. While there have been studies have considered the potential relationship between immune phenotypes and the response of ICI. However, so far it has not been studied that prediction of ICI response within immune phenotypes and which immune evasive processes underpin these immune phenotypes. An in-depth understanding the immune infiltrates within TME can provide valuable insights into the efficacy of ICI therapy. Immune infiltrates refer to the types and abundance of immune cells present in the tumor. Different immune cell populations play important roles in the anti-tumor immune response. The objective of researchers is to uncover

distinct immune phenotypes that are correlated with a favorable response to ICI treatment through the analysis of immune infiltrates. This can facilitate the advancement of predictive biomarkers to tailor treatment strategies to individual patients with diversity immune phenotypes. In summary, the predicting responsiveness to ICI based on immune phenotypes and tumor immune infiltrates is crucial for personalized treatment. This approach optimizes outcomes, avoids unnecessary treatments, enhances clinical trial design, and advances research in the field of cancer immunotherapy. By identifying which patients are likely to respond to a particular treatment, predictive biomarkers play a significant role in optimizing the use of therapies, improving patient outcomes, and minimizing unnecessary exposure to treatments with limited efficacy. This personalized approach to treatment based on predictive biomarkers re-envision the approach to tailoring therapy for cancer.

II. MATERIALS AND METHODS

1. Data acquisition

In the study, a comprehensive collection of 937 samples comprising seven distinct types of malignancies was obtained from nine publicly available databases (**Table 1**). The samples consist of either patient-specific immune phenotype obtained through IHC or information about the response to ICI therapy. There are two datasets, resource number EGAD00001003977 (cohort A and B, urothelial cancer) and Moffitt center (cohort C, clear cell renal cell carcinoma), which include both immune phenotype and ICI responsiveness information that is essential for the study to predict immune phenotype-specific responses^{9,19}. The EGAD00001003977 dataset consists of 337 samples, which were divided into two cohorts, namely cohort A and cohort B. The cohort A with 182 samples and cohort B with 62 samples were divided using stratified sampling with a ratio of 0.75 to 0.25.

In order to predict the immune phenotype, six previously used datasets were employed, including an overall count of 809 samples gathered from five cancer types (**Table 2**). From these, 621 samples with immune phenotype information collected from five public data were used as training set for immune phenotype classification. The training set consists of cohort A with and cohort C with both ICI responsiveness and immune phenotype information, as well as cohort E (Moffitt center) with 84 samples and cohort F (EGAD00001004988) with 350 ovarian samples, including only immune phenotype information²⁰. The test set for the immune phenotype classification model comprised a total of 101 samples, sourced from cohorts B and C consisting of urothelial cancer patients. For independent validation, I compiled 87 samples from three distinct datasets. This validation set incorporates 15 ovarian cancer patients from cohort G (EGAD00001006975), 51 melanoma patients from cohort H (PRJNA715643), and 21 colorectal cancer patients from cohort I (PRJNA727917)²¹⁻²³.

For determining the immune phenotype-specific response to ICI, six publicly

data resources were utilized (**Table 3**). These datasets collectively comprised 377 samples, which were gathered across five different cancer types. A combined total of 187 samples with immune phenotype and ICI responsiveness information from cohort A and cohort C were used as the training set for immune phenotype-specific ICI response prediction. And 62 samples from cohort B were applied as a test set. To verify immune phenotype-specific ICI response predictive models, the 128 samples were obtained from three cancer types consisting of cohort J from melanoma (ERP105482, $n = 41$), cohort K from gastric cancer (ERP107734, $n = 45$), cohort L from lung cancer (SRP183455, $n = 16$) and cohort M from lung cancer (SRP217040, $n = 26$) as independent validation datasets with only ICI response information²⁴⁻²⁷.

Table 1. Cohort information of the study

Cohort	Clinical Information	Cancer Type	Sample Count	Resource
Cohort A	Immune Phenotype & ICI response	Urothelial	182	EGAD00001003977
Cohort B			62	
Cohort C		ccRCC	5	Moffitt center
Cohort D		Urothelial	39	EGAD00001003977
Cohort E		ccRCC	84	Moffitt center
Cohort F	Immune Phenotype	Ovarian	350	EGAD00001004988
Cohort G			15	EGAD00001006975
Cohort H		Melanoma	51	PRJNA715643
Cohort I		Colorectal	21	PRJNA727917
Cohort J		Melanoma	41	ERP105482
Cohort K	ICI response	Gastric	45	ERP107734
Cohort L			16	SRP183455
Cohort M		Lung	26	SRP217040
7 cancer types			937	9 public datasets

Table 2. Data for immune phenotype classification

Data Type	Cohort	Cancer Type	Sample Count
Training (n=621)	Cohort A	Urothelial	182
	Cohort C	ccRCC	5
	Cohort E		84
	Cohort F	Ovarian	350
Test (n=101)	Cohort B	Urothelial	62
	Cohort D		39
Validation (n=87)	Cohort G	Ovarian	15
	Cohort H	Melanoma	51
	Cohort I	Colorectal	21

Table 3. Data for immune phenotype-specific ICI response prediction

Data Type	Cohort	Immuno-therapy	Cancer Type	Sample Count
Training (n=187)	Cohort A	Anti-PDL1(Atezolizumab)	Urothelial	182
	Cohort C	Anti-PD1 (Nivolumab)	ccRCC	3
		Anti-PD1 (Pembrolizumab)		2
Test (n=62)	Cohort B	Anti-PDL1(Atezolizumab)	Urothelial	62
Validation (n=128)	Cohort J	Anti-PD1 (Pembrolizumab)	Melanoma	33
		Anti-PD1 (Nivolumab)		8
	Cohort K	Anti-PD1 (Pembrolizumab)	Gastric	45
	Cohort L	Anti-PD1 (Nivolumab)	Lung	16
	Cohort M	Anti-PD1 (Nivolumab)	Lung	26

2. Quantification of gene expression from bulk RNA sequencing

To calculate gene expression from bulk RNA sequencing data of samples, transcriptome reads were aligned to the human reference using Spliced Transcripts Alignment to a Reference (STAR, version 2.7.9a), and gene expression values were quantified using RSEM (version 1.3.1) with GENCODE (version 39) annotation data^{28,29}. For normalized read counts, the gene length is calculated using the annotation by GENCODE. The normalized read count for each gene was converted to Transcript Per Million (TPM). In addition, we employed a RNA-Seq normalization technique known as Gene length corrected trimmed mean of M-values (GeTMM) to get the expression values to enable comparisons between and within sample via edgeR package^{30,31}.

3. Estimation of immune phenotype specific ICI response

The raw read count is adjusted for differential expression analysis with ComBat-seq and RUVseq, which are used to remove unwanted variation and batch effects from cohorts^{32,33}. The adjusted read count of each gene was normalized using the DESeq2 to enable comparisons between immune phenotype-specific ICI response groups³⁴. These ICI response groups were aptly named as the 'Responder' (R) group, comprising patients exhibiting either a complete (CR) or partial response (PR), and the 'Non-Responder' (NR) group, incorporating those with stable disease (SD) or progressive disease (PD). The differentially expressed genes (read count ≥ 3 , $|\log\text{FC}| \geq 1$ and $0.05 > P_{\text{adj}}$) were inferred between the R and NR groups for each immune phenotype of ICI treatment. The classifier gene-set of immune phenotype specific ICI response with different expression patterns in the responders compared to nonresponders in each immune phenotype of cohort A was chosen using differential gene expression (DE) analysis.

Subsequently, I adopted elements of the wilcoxon rank sum test concept to conduct intergroup comparative analysis. I calculated the Total Rank for the DEGs obtained from each phenotype from training dataset within both the ICI response and non-response groups. Then, I calculate the ratio of the total ranks between the upregulated genes in response group (RGs) and the upregulated genes in non-response group (NRGs) and establish a set of standard answers to compare with unknown samples based on that ratio of total rank value.

$$\text{Ratio of total rank} = \frac{\sum \text{Rank of RGs}}{\sum \text{Rank of NRGs}}$$

The Median Absolute Deviation (MAD) is a robust measurement used to compare the ratio of total ranks between ICI response groups. MAD calculates the average distance between each data point and the median of a dataset.

Following this, I compared the differential in MAD values when the unknown sample was included in the standard answer sets of each the response and non-response groups, to predict the ICI responsiveness of the unknown sample. By determining the group with the lowest differential MAD between responders and non-responders, I can predict the ICI responsiveness of the unknown sample. A lower differential MAD suggests that the unknown sample's immune phenotype align more closely with the traits exhibited by either the response or non-response group, indicating its potential ICI response. This approach allows for an objective evaluation of the unknown sample's ICI responsiveness, providing insights and predictions based on the observed changes in MAD values within the response and non-response groups. The CLIPS is available at <https://github.com/hellokeyworld/CLIPS>.

4. Collection of immune phenotype specific features

A. Prevalence of immune cell type

The estimated immune cell fractions of the bulk RNA sequencing were determined using the normalized TPM of each gene. The EPIC module in `immunedonv` was used signature matrix designed and validated to

quantify 8 different immune cell types for each sample^{35,36}. The absolute value of immune cell fractions evaluated by EPIC allows inter-and intra-sample comparisons and used reference gene expression profiles for various cell types validated low cytometry, and immunohistochemistry data. The absolute values of immune cells received from quantiseq were used to calculate the ratio value and then employed as a model generation feature to compare the relative distribution among immune cells.

B. The fraction of stromal and immune cells

The tumor environment is inferred by using the ESTIMATE score based on the level of infiltrating stromal and immune cells by single-sample gene set-enrichment analysis (ssGSEA) on the stromal and immune signatures³⁷. These scores for each sample are calculated based on gene expression data derived from RNA sequencing. In this study, the ESTIMATE provided in the R package was used. The estimate score is indicative of tumor purity, while the stromal score reflects the presence of stromal components in tumor tissue. Additionally, the immune score quantifies the level of immune cell infiltration within the tumor.

C. Immune phenotype related gene

Organize the expression of genes contained in the immune phenotype related gene or cancer-immunity cycle that can affect the immune phenotype through literature research. From these prior investigations, I was able to extract 47 gene datasets and 156 gene sets linked to immune phenotypes^{20,38}. To build the classification model, the geomean value of the expressed genes from the dataset was computed.

Next, six features related to gene expression associated with immune phenotypes, were gathered alongside seven Tumor Inflammation Signature (TIS) scores, four Immune Profiling System (IPS) scores, and Cancer-Immunity Cycle (CYT) scores for the purpose of immune phenotype classification³⁹⁻⁴¹.

5. Classification model of immune phenotype

The training datasets for models that classify immune phenotypes are cohort A, cohort C, cohort E and cohort F. The training dataset consists of 209 inflamed immune phenotype, 203 excluded immune phenotype and 217 desert immune phenotype. This study utilized a multi-classification algorithm to construct a model capable of distinguishing among three immune phenotypes with k-fold cross validation. Five multi-class classification algorithms—KNN, Regression Tree, Random Forest, Naïve Bayes, and Support vector machines (SVM)—were developed for the classification of immune phenotypes. In order to differentiate between three immune phenotypes, a model was constructed by employing the KNN algorithm within a multi-class classification framework. All features used for building the model were min-max scaled. The immune cell deconvolution process was used to the bulk RNA sequencing data to infer the patient's TME of immunological environment. The immune phenotype classification model was evaluated using 101 samples from cohort B and cohort D as the test dataset, while 87 samples from cohort G, cohort H and cohort I were used as independent validation datasets to verify the model's accuracy.

6. Generation of TIDE and IMPRES score

In the next step, the performance comparison between CLIPS (Classification of Immune Phenotypes-Specific ICI response), Tumor Immune Dysfunction and Exclusion (TIDE), and IMmuno-PREdictive Score (IMPRES) was conducted in the context of providing responsive predictions for ICI treatment using RNA sequencing data^{42,43}. The TIDE algorithm was applied in order to tailor response estimates to each specific cancer type. The IMPRES score, typically ranging from 0 to 15, provides a numerical representation of the patient's immune response. Patients with higher IMPRES scores may be more

likely to respond to immunotherapies. So, we used the TIDE to customize the response estimate for each cancer type and classified values above 9 for IMPRES as ICI response groups.

7. Gene set enrichment analysis

Gene Set Enrichment Analysis (GSEA) was performed on a list of genes with differences in gene expression between immune phenotype-specific ICI responsiveness groups.

To identify of key biological processes that are relevant to the research, I used the Hallmark gene set with version h.all.v2023.1.Hs.symbols collected from the Human Molecular Signatures Database (MSigDB)⁴⁴.

The GSEA analysis was performed with the R package fgsea (Fast Gene Set Enrichment Analysis) with v1.26.0⁴⁵. Pathways having a minimum of 5 or more genes were considered, and permutation was done 1,000 times. Only pathways with a adjusted p-value of 0.1 or below have been determined to be significant and included in the analysis.

8. Statistical analysis

The overall statistical analysis was performed using R version 4.3. Multiple testing correction was performed for differential gene expression analysis using the Benjamini- Hochberg method. The Kruskal–Wallis test was used to evaluate differences in gene expression and immune cell proportions between immune phenotypes and immune phenotype-specific ICI response groups. For time-to-event analysis, I used the R survminer package v0.4.9 to generate Kaplan–Meier (KM) plots and calculate log-rank p-values.

III. RESULTS

1. Expression of *PD-1* and *PD-L1* in relation to immune phenotype and ICI response

The *PD-1* inhibitor and *PD-L1* inhibitor enhance the ability of immune cells to recognize and eliminate tumor cells by disrupting the interaction between *PD-1* and *PD-L1*. Consequently, the ability of immune cells to recognize and eliminate tumor cells is enhanced, reducing the likelihood of cancer cells evading the immune response. Moreover, PD-L1 functions as a significant cancer biomarker since higher levels of PD-L1 expression are associated with improved results in immunotherapy⁴⁶.

Prior studies have discovered that when examining samples taken before therapy with anti-PD-1 and anti-PD-L1, there was a notably substantial abundance of CD8+T cells near the invasive margin in individuals who responded positively to the treatment⁴⁷. Additionally, serial sampling during treatment demonstrated an increased infiltration of CD8+T cells into the tumor parenchyma.

Conversely, analysis of the EGAD00001003977 resource dataset, encompassing cohorts A and B, demonstrates a uniformity in immune phenotype distribution with no notable variances in ICI response (**Figure 2A**, fisher test p-value = 0.403). Consequently, this dataset is well-suited for the investigation of potential correlations between immune phenotypes and ICI responses at the genetic level. The observations in this study indicate no significant difference in *PD-1* and *PD-L1* expression following ICI response (**Figure 2B** and **Figure 2C**, wilcoxon test p-value 0.53 and 0.19). However, significant variations are observed in immune phenotypes when considering *PD-1* and *PD-L1* expression levels (kruskal test p-value 1.74e-13 and 8.19e-13).

These findings indicate that the *PD-1* and *PD-L1* expression levels were higher in the inflamed immunophenotype and lowered in the excluded and desert

phenotypes. Consequently, the expressions of *PD-1* and *PD-L1* are linked to the immune phenotype. As highlighted in earlier research, the inflamed immune phenotype tends to respond favorably to ICI treatment.

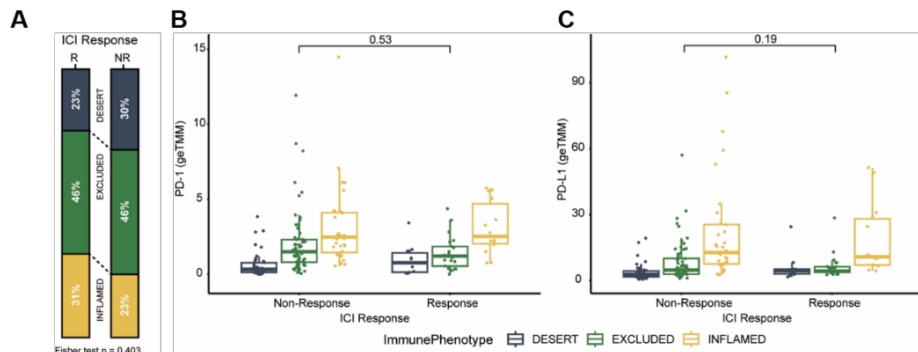


Figure 2. The association between the immune phenotype and ICI response.

(A) Distribution of immune phenotype and ICI response. The yellow indicates inflamed immune phenotype, green indicates excluded immune phenotype and blue indicates desert immune phenotype. (B) ICI response and immune phenotype in relation to *PD-1* and (C) *PD-L1* expression.

2. Overview of CLIPS

The objective of study is to develop a computational model called CLIPS (Classification of Immune Phenotypes-Specific ICI response), which works with patient RNA sequencing data to predict the response to immune checkpoint inhibitors (ICI) based on immune phenotype. CLIPS features three distinct operational modes for predicting the response to ICI tailored to specific immune phenotypes, each differentiated by its approach to managing immune phenotype information (**Figure 3**).

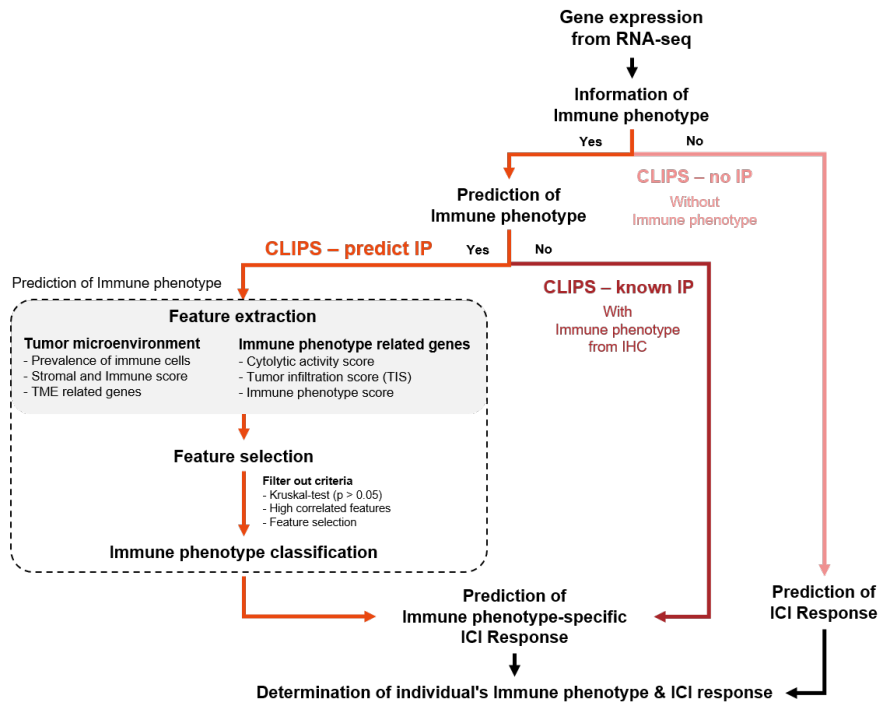


Figure 3. Overview of CLIPS.

The process demonstrates predicting patient-specific immune phenotype and immune phenotype-specific ICI response through CLIPS from RNA sequencing data. The red color represents the known IP (immune phenotype), the orange represents the predict IP, and the pink represents the no IP.

The first mode, CLIPS–known IP, represents a robust predictive model for ICI response, which relies on the patient specific immune phenotype information

gathered via IHC. The second mode, CLIPS–predict IP, employs the immune phenotype information predicted by CLIPS to accurately predict the responsiveness to ICI, rather than relying on the direct immune phenotype data obtained by IHC. Lastly, CLIPS–no IP offers a predictive method to determine patient reactivity to ICI without the need for immune phenotype information. All three modes of CLIPS demonstrate superior performance compared to the conventional methods, TIDE and IMPRES, in the test set (cohort B). The accuracy values were measured using the CLIPS, TIDE, and IMPRES methods, with results of 0.79 for CLIPS–known IP, 0.74 for CLIPS–predict IP, 0.56 for CLIPS–no IP, 0.53 for TIDE, and 0.26 for IMPRES.

A. Classification of immune phenotype

A comprehensive set of 28 features pertaining to the tumor microenvironment (TME) and the immune phenotype is used for the purpose of classifying the immune phenotype. Within the set of 28 features, one was dropped as they showed no variation across different immune phenotypes, and six were removed because of their high similarity to other features. Then, in the process of model selection, a total of 21 features were considered. Subsequently, feature selection was utilized to streamline the model by reducing the number of features from 21 to 16, enhancing performance and mitigating the possibility of overfitting. After careful evaluation and analysis, it was decided to include only 16 of these features in the final multi-class classification model. The selected features can be identified in **Figure 4** as differences between the individual immune phenotype.

Five distinct multi-class classification algorithms have been developed and subjected to comprehensive performance evaluations. The KNN (K-Nearest Neighbor) model selected for the classification of immune phenotype multi-class has high accuracy and AUC of 0.76 (**Figure 5**).

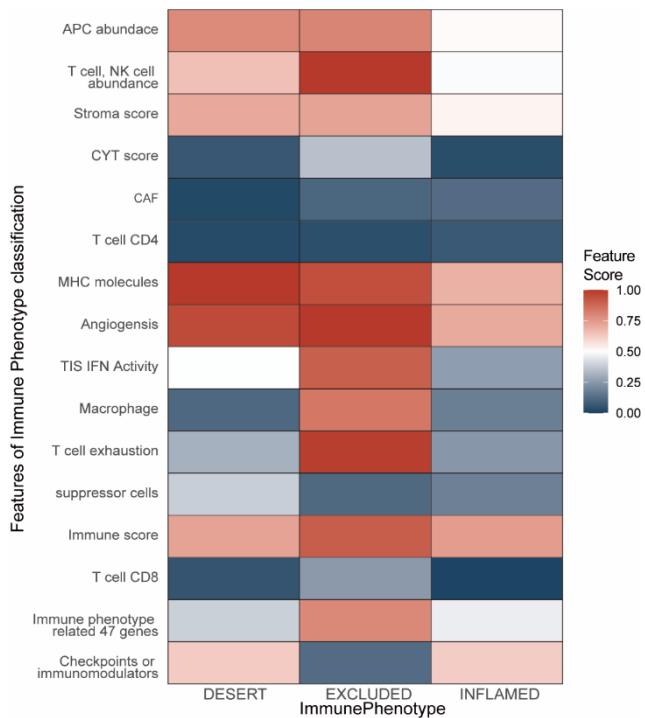


Figure 4. Selected 16 features for immune phenotype classification.



Figure 5. Performance of five immune phenotype multi-class classification. Comparing the performance of five multi-class classification algorithms on KNN, Regression tree, Random forest, Naïve bayes and SVM.

B. Prediction of immune phenotype-specific ICI response

The study utilized gene expression data obtained through RNA sequencing from patients in order to predict the responsiveness of ICI towards specific immune phenotypes. To enhance the precision of these predictions for ICI responsiveness, the analysis focused on comparing differentially expressed genes (DEG) between the responder group (R) and the non-responder group (NR) within each immune phenotype (**Figure 6**). To ensure specificity, DEGs shared amongst the three immune phenotypes were omitted from the individual lists of DEGs associated with each immune phenotype.

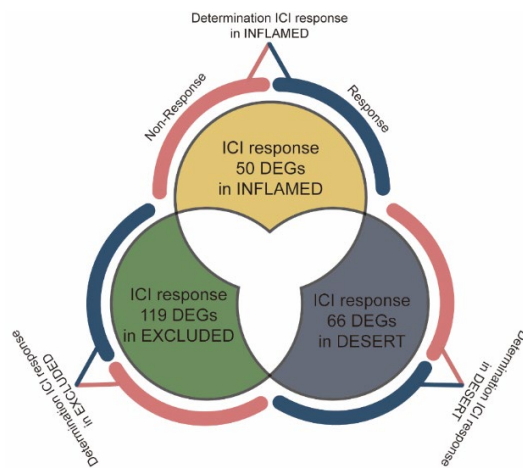


Figure 6. Prediction of immune phenotype-specific ICI response based on DEGs.

The classification of ICI response was performed on a set of 50 genes in the inflamed immune phenotype, 119 genes in the excluded immune phenotype, and 66 genes in the desert immune phenotype to determine the potential responsiveness of ICI. The heatmap analysis reveals distinct variations in the DEGs across immune phenotypes within the groups responsive to ICI (**Figure 7**).

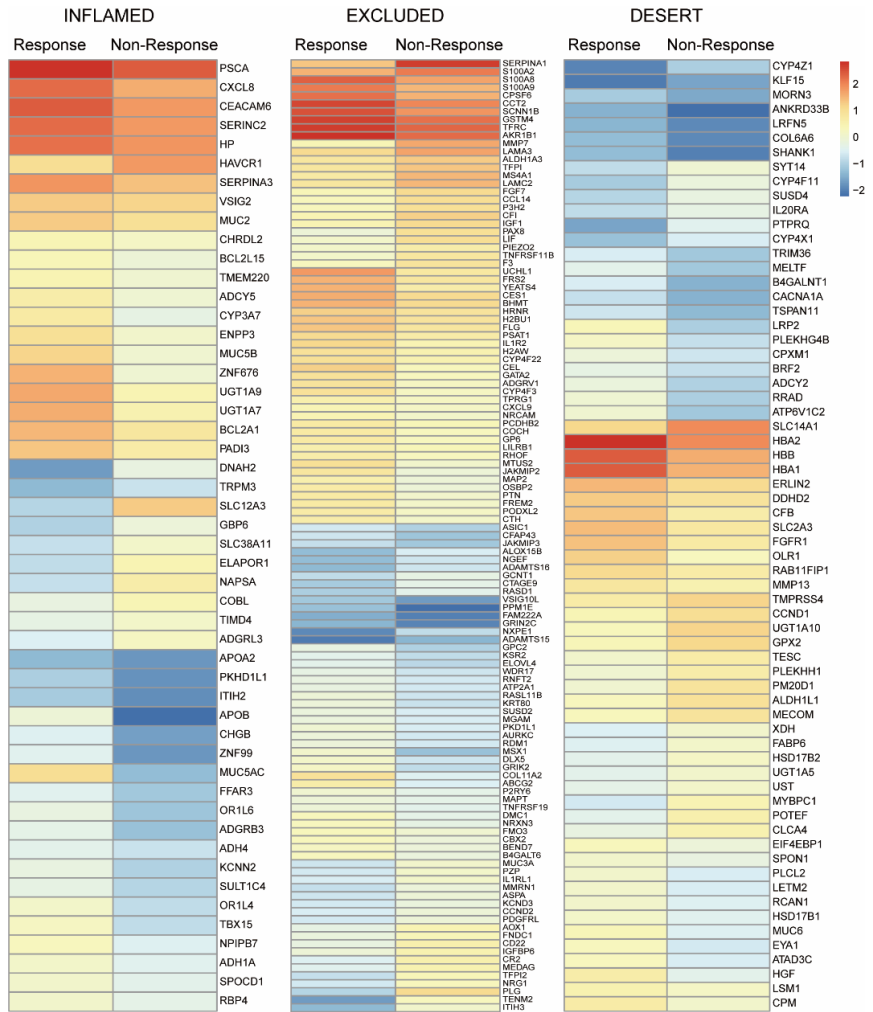


Figure 7. Heatmap of DEGs from immune phenotype-specific ICI response groups.

(Left) Heatmap of 50 DEGs from inflamed-specific ICI response group (Middle) 119 DEGs form excluded-specific ICI response group (Right) 66 DEGs from desert-specific ICI response group.

The ratio of total rank was compared within each immunophenotype among the ICI response groups (**Figure 8**). The average value of the ratio of the total rank for the NR group with ICI therapy across all immune phenotypes is greater than 1, with desert at 1.42, excluded at 1.09, and inflamed at 1.34. Meanwhile, the average ratio of the total rank for the ICI response group is comparatively low across immune phenotypes: 0.85 for desert, 0.79 for excluded, and 1.11 for inflamed. This comparison revealed statistically significant differences in immune phenotypes, suggesting that future predictions of sample ICI response could be made with high accuracy.

After that, to ensure the robustness of the DEGs based on immune phenotype-specific ICI responses, an analysis was conducted to determine whether differences existed across melanoma (cohort J), gastric cancer (cohort K), and lung cancer (cohort L and M). The analysis revealed no significant difference in the expression levels of total DEGs among melanoma, gastric cancer and lung cancer (**Figure 9A**, kruskal test p-value 0.21). Upon closer inspection, it becomes evident that there is no significant difference in the expression of DEGs associated with the inflamed and the desert immune phenotype among the different carcinomas(**Figure 9B and Figure 9D**). In the case of DEGs from excluded immune phenotype, it shows lower expression in gastric cancer compared to other cancers, but there is no difference in expression between lung cancer and melanoma (**Figure 9C**, kruskal test p-value 0.55).

This implies that these specific sets of genes related to the immune response are consistently expressed across various cancers without exhibiting any notable variation. This information suggests that the genetic characteristics underlying the immune phenotypes share similarities in the context of different cancer types.

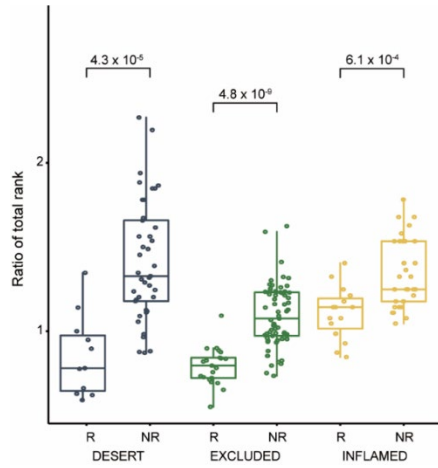


Figure 8. The ratio of total rank within ICI response.

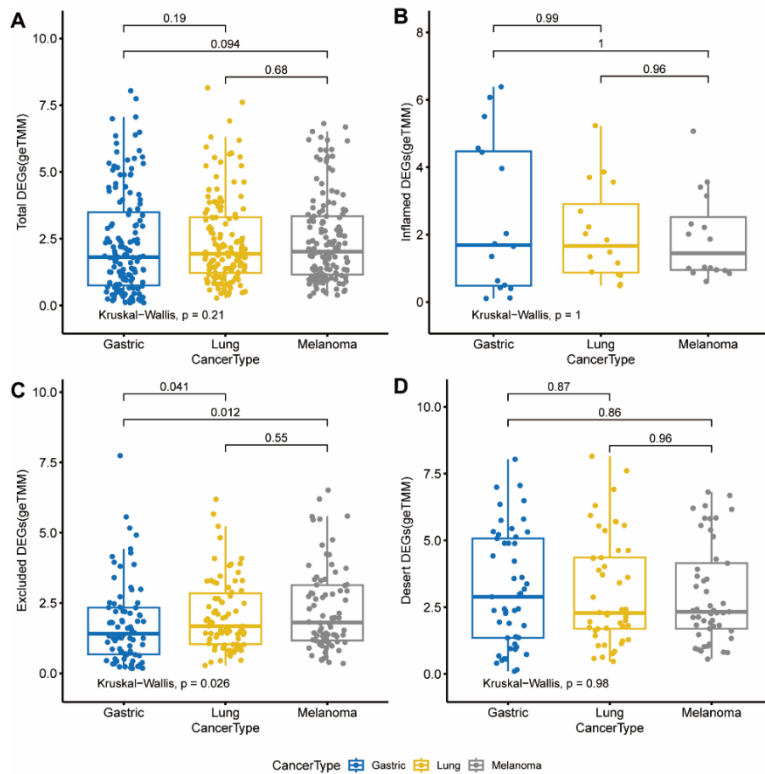


Figure 9. Comparison of ICI response DEGs according to cancer types.

3. Expression of *PD-1* and *PD-L1* in predicted immune phenotypes

Analysis of an independent validation dataset (cohort J,K,L and M) to determine if there are differences in the distribution of patient-specific immune phenotypes predicted through CLIPS based on ICI responsiveness groups showed that the inflamed immune phenotype is more prevalent in the R group across the entire validation set (**Figure 10A**, fisher test p-value $2.4e-6$).

Upon examination by cancer type, the incidence of the inflamed immune phenotype was found to be 27% in the NR group and over 75% in the responsive group for melanoma and lung cancer. This highlights a significant disparity between the ICI response groups. In the case of gastric cancer, although not statistically significant, a noteworthy finding was that 92% of the R group exhibited the inflamed phenotype, while the excluded phenotype was absent.

Furthermore, I investigated the association between the expression of *PD-1* and *PD-L1* mentioned in Result 1, and the ICI response groups and immune phenotypes predicted through CLIPS (**Figure 10B** and **Figure 10C**). The results of this study showed that both *PD-1* and *PD-L1* demonstrate significantly higher expression levels in the inflamed immune phenotype compared to other immune phenotypes. Also, a statistically significant distinction was identified between the R and NR groups of ICI treatment, wherein the responsive group had elevated levels of *PD-1* and *PD-L1* expression (wilcoxon test p-value $5.2e-6$ and $3.4e-6$). These results prove an association between *PD-1* and *PD-L1* expression and immune phenotypes. Increased gene expression levels of *PD-1* and *PD-L1* can indicate the presence of an inflamed immune phenotype.

The results of this research add to the expanding understanding of the complex relationship between immune phenotypes and the expression of *PD-1* and *PD-L1* in relation to the effectiveness of ICI.

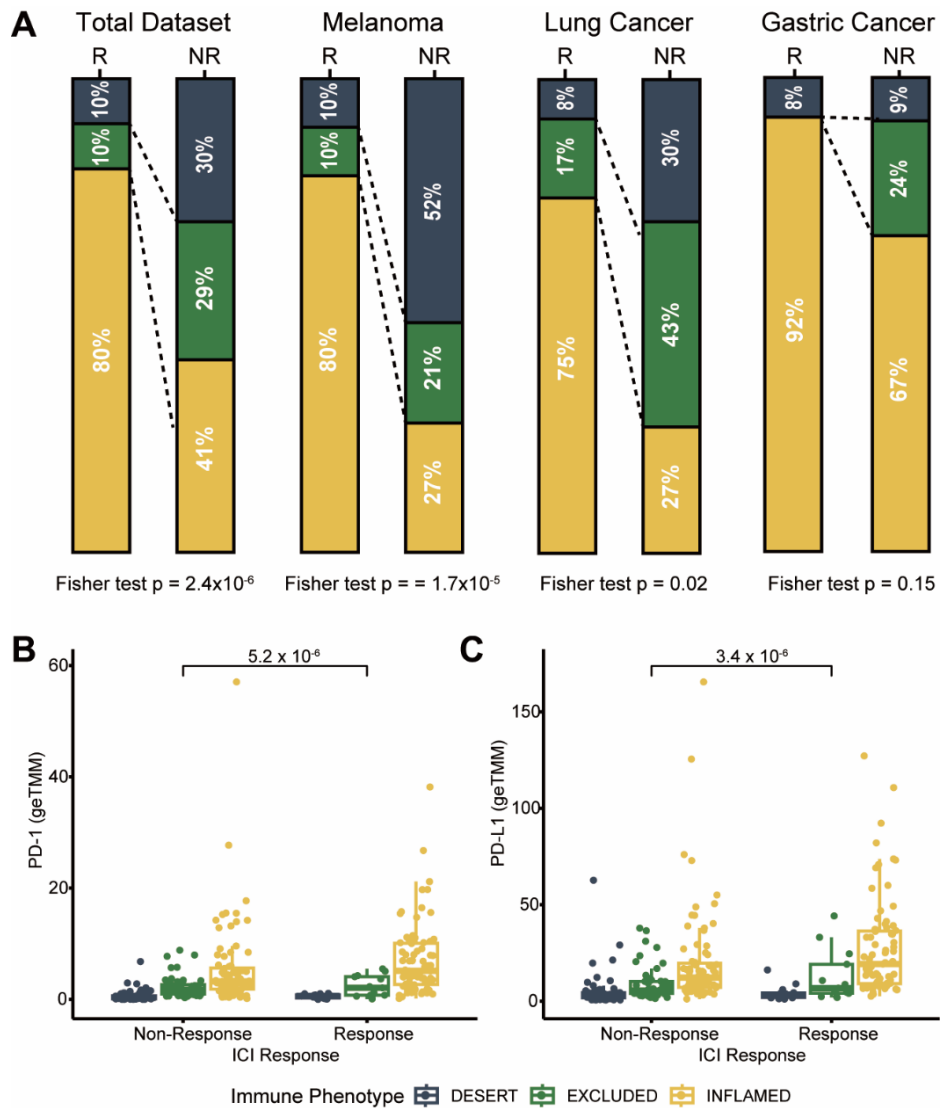


Figure 10. The association between the ICI response and predicted immune phenotype from CLIPS.

(A) Distribution of predicted immune phenotype and ICI response in validation dataset according to cancer types. (B) ICI response and predicted immune phenotype in relation to *PD-1* and (C) *PD-L1* expression.

4. Overall survival

The effect of ICI therapy responsiveness on patients' overall survival has been well established through previous studies⁴⁸. The group that shows response to ICI treatment has a longer overall survival compared to the group that does not respond. This finding has also been confirmed in the separate validation dataset used in this study, which also verified its significance in melanoma and lung cancer (Figure 11 A-C).

The patient's overall survival can be influenced by both the response to ICI treatment and immune phenotypes³. An analysis of immune phenotypes anticipated using CLIPS to determine their impact on overall survival revealed that the inflamed immune phenotype was correlated with improved survival (Figure 11D). Upon additional analysis based on the type of cancer, it was shown that in melanoma, those with the inflamed phenotype had a significantly higher median overall survival of 700 days compared to those with the other two immune phenotypes (Figure 11E). In gastric cancer, although no statistical difference was found between the immune phenotypes, the inflamed phenotype was observed to have a higher median overall survival value (Figure 11F).

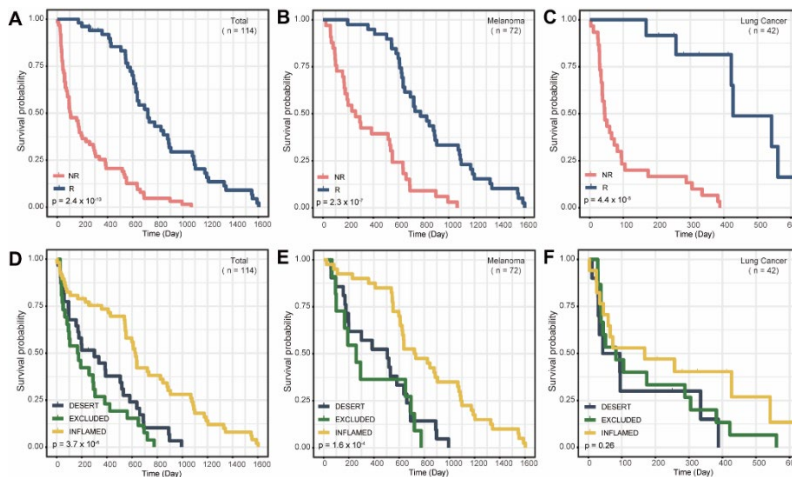


Figure 11. Overall survival analysis according to ICI response and immune phenotypes.

5. Evaluation of CLIPS for ICI response prediction

A. Performance evaluation in test dataset

A comparison was made between the currently utilized methodologies to evaluate the performance of CLIPS for ICI response prediction. The TIDE and IMPRES are known as two approaches to be effective in predicting the responsiveness of ICI.^{42,43}

To compensate for the instability from the dataset, I compared the performance of three modes of CLIPS, TIDE, and IMPRES with a total of five prediction tools using MCC (Matthews correlation coefficient) and Accuracy⁴⁹. A performance comparison of the models within test dataset (cohort B) showed that the CLIPS-known IP model achieved an accuracy of 0.79, the CLIPS-predict IP attained an accuracy of 0.74, and the CLIPS-no IP reached an accuracy of 0.56. The TIDE recorded an accuracy of 0.53, while the IMPRES had an accuracy of 0.26 (**Figure 12**).

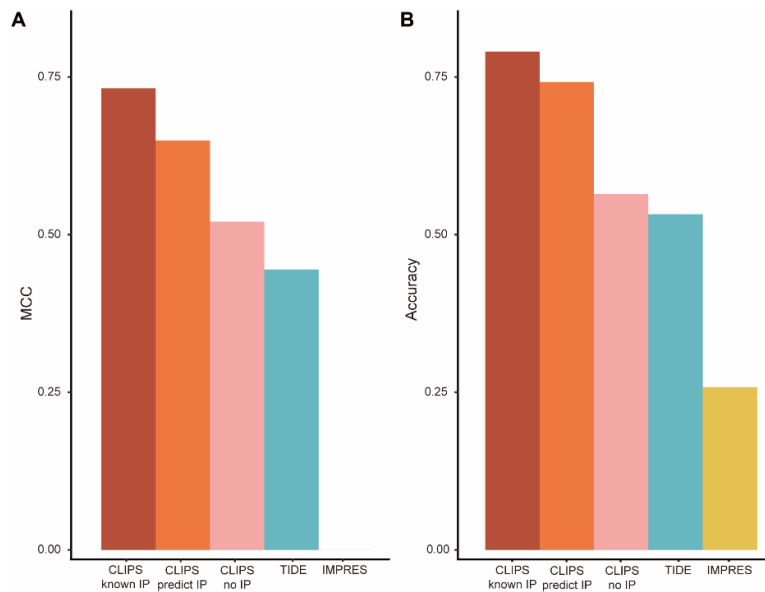


Figure 12. Comparison of the performance of five ICI response prediction tools with MCC and Accuracy in test dataset.

To conduct a comprehensive performance evaluation, I calculated eight performance evaluation indicators, namely MCC, Accuracy, F1 score, Area Under the Curve (AUC), Sensitivity (Recall), Specificity, Precision (PPV), and Negative Predictive Value (NPV). CLIPS-known IP and CLIPS-predict IP outperforms conventional methods, TIDE and IMPRES, across seven performance measures in the test dataset (**Figure 13**). The IMPRES tool exhibits a sensitivity value of 1, indicating a high rate of correctly identified positive cases compared to other tools. However, it also has a specificity of 0, indicating a lack of correctly identified negative cases. This suggests an imbalance in the prediction performance of the IMPRES, as it tends to prioritize sensitivity at the expense of specificity.

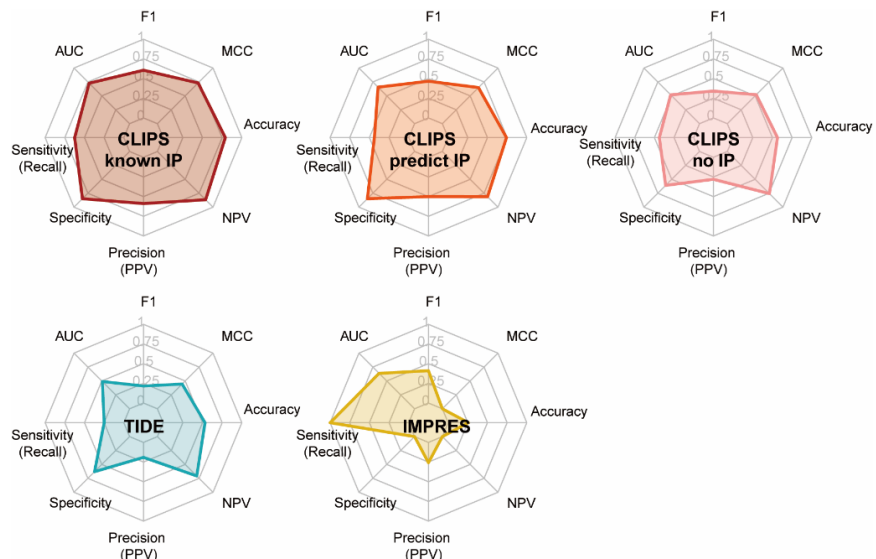


Figure 13. Comparison of the performance of five ICI response prediction tools with all performance measures in test dataset. The radar plot displays the performance parameters for each ICI response prediction tool, with larger colored areas indicating superior all-around performance.

Furthermore, I analyzed whether there were differences in predicting ICI response even within the immune phenotypes. For each prediction tools of TIDE, IMPRES and CLIPS, I checked for bias in prediction based on immune phenotypes in test dataset (**Table 4**). In the test dataset consisting of 62 samples, there are 16 samples with inflamed immune phenotype, 18 samples categorized as excluded, and the remaining 28 samples are characterized by desert immune phenotype. In the examination of different immune phenotypes, CLIPS consistently showed better predicting ability than conventional methods. (**Table 5**). Although inflamed and desert immune phenotypes exhibited similar levels of predictive performance, it was noted that all ICI response prediction tools as TIDE, IMPRES, and CLIPS showed a relative decline in predictive performance for immune phenotypes assigned as excluded. Indeed, through rigorous evaluation and analysis, it has been demonstrated that the CLIPS model possesses a remarkable capability to accurately predict ICI response.

Table 4. Confusion matrix of test dataset within immune phenotype

Prediction Tool	Predicted ICI response	Total		INLFMAED		EXCLUDED		DESERT	
		Actual R (PR+CR)	Actual NR (SD+PD)						
CLIPS-known IP	R	10	7	3	2	2	2	5	3
	NR	6	39	2	9	2	12	2	18
CLIPS-predict IP	R	7	7	3	3	2	2	2	2
	NR	9	39	2	6	4	13	3	20
TIDE	R	4	17	1	3	0	5	2	7
	NR	12	29	4	8	4	9	5	14
IMPRES	R	16	46	5	11	4	14	7	21
	NR	0	0	0	0	0	0	0	0

Table 5. Performance indicator in immune phenotypes from IHC

Immune					
Phenotype from IHC	Predicted Tool	MCC	Accuracy	F1 score	AUC
INFLAMED	CLIPS-known IP	0.709	0.750	0.600	0.709
	TIDE	0.461	0.563	0.222	0.464
	IMPRES	0	0.313	0.476	0
EXCLUDED	CLIPS-known IP	0.679	0.778	0.500	0.679
	TIDE	0.334	0.500	0	0.346
	IMPRES	0	0.222	0.364	0
DESERT	CLIPS-known IP	0.774	0.821	0.667	0.763
	TIDE	0.478	0.571	0.25	0.48
	IMPRES	0	0.25	0.4	0

B. Performance evaluation in independent validation dataset according to anti-PD-1 treatment

In order to evaluate the predictive performance, I utilized standard prediction tools, TIDE and IMPRES, along with CLIPS, on an independent validation dataset with 128 samples (cohort J-M). To handle the lack of immune phenotype information in the independent validation dataset, two CLIPS models were chosen for analysis. The first model, called CLIPS–predict IP, used predicted immune phenotypes to forecast the response to ICI. The second model, CLIPS–no IP, was specifically designed to predict ICI response without relying on any immune phenotype information.

The analysis aimed to determine if there were any variations in the performance of CLIPS's prediction of ICI responsiveness based on the specific type of anti-PD1 treatment. The study analyzed a total of 128 samples from patients who received anti-PD1 treatment with Nivolumab or Pembrolizumab. According to the total data, the MCC of the CLIPS–prediction IP was 0.70 and the Accuracy was 0.72. This indicates that the CLIPS–predict IP outperformed other tools in terms of both MCC and Accuracy (**Figure 14A** and **Figure 14D**). TIDE showed the second highest performance after CLIPS–predict IP with MCC of 0.60, and Accuracy of 0.65. Lastly, the performance of IMPRES and CLIPS–predict IP is lower than 0.6. In CLIPS–predict IP, in addition to Accuracy and MCC, eight performance predictor indicators can identify large areas of good performance with relatively high values (**Figure 15A**).

Following that, for 50 patients treated with Nivolumab (cohort J, L and M), one of the anti-PD1 methods, CLIPS was more accurate than the other methods with MCC of 0.71 and Accuracy of 0.72 (**Figure 14B** and **Figure 14E**). Also, CLIPS generally has high values in other performance indicators, with sensitivity 0.73 and specificity 0.71 (**Figure 15B**). This

suggests that CLIPS may be particularly effective in predicting the response to Nivolumab treatment in this group of patients.

Subsequently, the 78 patients received with Pembrolizumab known as the biomarker for *PD-L1* expression and worked on performance assessments in cohort J and cohort K, an independent validation dataset consisting of other tumors type. The CLIPS–predict IP model achieved an accuracy of 0.72 and CLIPS–no IP model had an accuracy of 0.56. Meanwhile, the TIDE model recorded an accuracy of 0.63 and the IMPRES model had an accuracy of 0.40 (**Figure 14C** and **Figure 14F**). Comparison of other performance metrics reveals that IMPRES has a higher sensitivity of 0.96, which is greater than CLIPS–predict IP at 0.61 and TIDE at 0.50 (**Figure 15C**). Nevertheless, it has been noted that IMPRES is making imbalanced predictions with a specificity of just 0.08. Apart from this finding, CLIPS–predict IP is confirmed to have the highest values among the other performance measures.

Overall, the results of the analysis demonstrate the potential of CLIPS–predict IP as a predictive tool for determining the responsiveness to anti-PD1 treatment. By incorporating immunological characteristics, CLIPS–predict IP enhance the accuracy and reliability of reactivity predictions in the context of ICI.

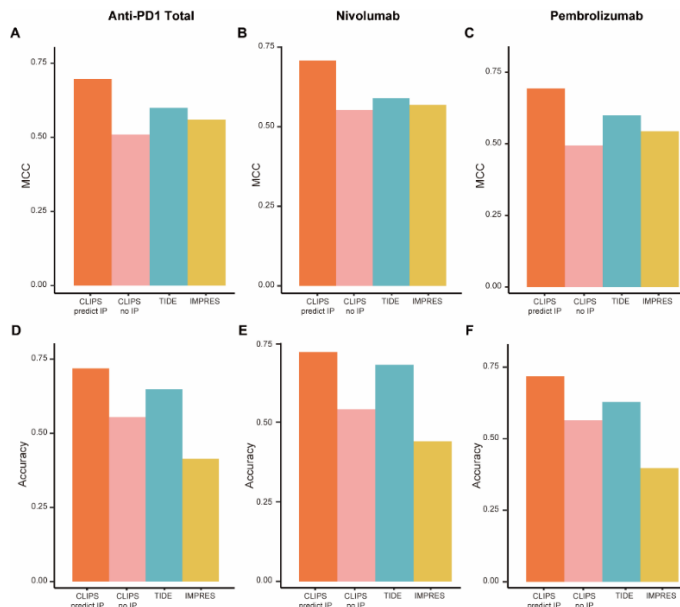


Figure 14. MCC and Accuracy within independent validation dataset according to anti-PD-1 treatment types.

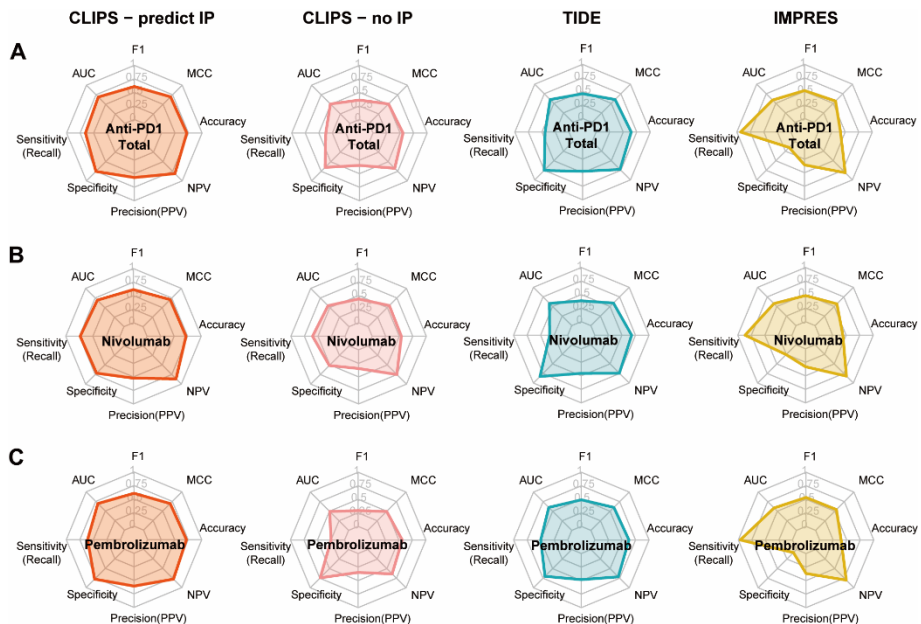


Figure 15. Performance evaluation for independent validation dataset according to anti-PD1 treatment types.

C. Performance evaluation in independent validation dataset within cancer types

The performance assessments were undertaken to predict the responsiveness to ICI for three different forms of cancer: melanoma, lung cancer, and gastric cancer. These assessments considered the heterogeneity observed within each type of cancer. The objective was to evaluate and compare the effectiveness of ICI treatment across these diverse cancer types, considering their unique characteristics and variations in treatment response.

The first analysis of 41 melanoma samples assessed the effectiveness of several prediction methods for predicting responses to ICI. The results indicated that CLIPS–predict IP emerged as the superior prediction tool, with an accuracy score of 0.76 and an MCC of 0.75, outperforming its competitors (**Figure 16A** and **Figure 16D**). CLIPS–predict IP has higher values in eight performance metrics compared to other prediction tools for ICI response (**Figure 17A**). Although, IMPRES shows a bias in its predictions with a sensitivity of 1 but a specificity of 0. On the other hand, CLIPS–predict IP is well-balanced prediction model with sensitivity of 0.74 and specificity of 0.77. This balance in sensitivity and specificity suggests that CLIPS–predict IP takes into account both non-responsiveness and responsiveness to ICI treatment, resulting in a more reliable and accurate prediction model.

Second, among the four prediction algorithms evaluated for 42 lung cancer patients from cohorts L and M, CLIPS exhibited higher accuracy compared to CLIPS–no IP, TIDE and IMPRES (**Figure 16B** and **Figure 16E**). CLIPS–predict IP achieved an MCC of 0.69 and an accuracy of 0.71. In contrast, CLIPS–no IP exhibited an MCC of 0.55 and an accuracy 0.55, TIDE showed an MCC of 0.55 and an accuracy of 0.71, while IMPRES had an MCC of 0.57 an accuracy of 0.45. These results indicate

that CLIPS–predict IP was the most accurate and yielded a higher MCC, suggesting better overall performance in predicting lung cancer outcomes for these patient cohorts. As with previous analyses, eliminating sensitivity and specificity, CLIPS–predict IP demonstrates higher predictive performance in comparison with other predictive tools (**Figure 17B**). Specifically, CLIPS–predict IP has a sensitivity of 0.67 and specificity of 0.73, while TIDE exhibits a sensitivity of 0.33 and specificity of 0.87, and IMPRES shows a sensitivity of 0.83 and specificity of 0.30. These findings indicate that both TIDE and IMPRES exhibit biased predictions.

As a final analysis, I evaluated predictive performance with 45 gastric cancer patient data from cohort J. The CLIPS-predict IP model attained an accuracy of 0.64, while its counterpart, the CLIPS-no IP registered an MCC of 0.62 and an accuracy of 0.64. In comparison, the TIDE model achieved an MCC of 0.63 and an accuracy of 0.64, and the IMPRES model had an MCC of 0.53 and an accuracy of 0.33 (**Figure 16C** and **Figure 16F**). For additional performance metrics, the precision value (PPV) for CLIPS-predict IP stands at 0.43, CLIPS-no IP at 0.30, TIDE at 0.40, and IMPRES at 0.28 (**Figure 17C**).

In summary, the large regions shown in **Figure 17** indicate that CLIPS–predict IP is more accurate than the other prediction models in forecasting patient response to ICI treatment across different kinds of cancer. Furthermore, CLIPS, unlike TIDE and IMPRES, takes a balanced approach to prediction by not only focusing on non-responsiveness to ICI or responsiveness, but considering both aspects. CLIPS is designed to provide accurate predictions for both response and non-response groups, resulting in a more comprehensive and well-rounded performance. Its balanced predictive performance makes CLIPS a valuable tool for determining the likelihood of response to ICI across a range of patients.

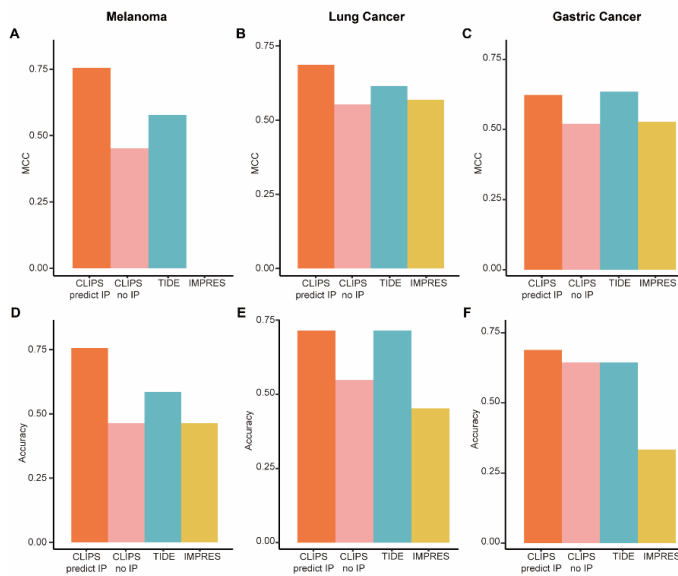


Figure 16. MCC and Accuracy within independent validation dataset according to cancer types.

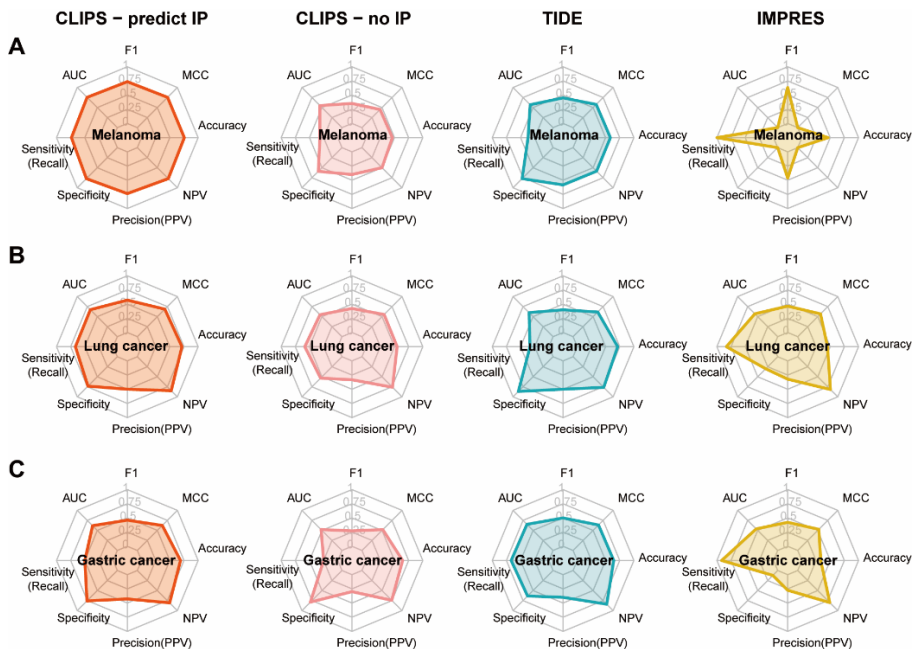


Figure 17. Performance evaluation for independent validation dataset according to cancer types.

6. Genomic characteristics of ICI response based on immune phenotype

The desert and excluded immune phenotypes are reported as not anticipated to respond to ICI treatment in previous research³⁸ However, in actual patient data like EGAD00001003977 data resource, ICI responsiveness from desert and excluded can be determined. Therefore, we would like to contribute to the ICI response prediction method by investigating the genetic characteristics of patients who respond to ICI in excluded and desert immune phenotypes. **(Figure 18)**

In the desert and excluded immune phenotypes, the Gene Set Enrichment Analysis (GSEA) focusing on over-expressed genes in patients who responded to ICI therapy compared to non-responders has provided evidence of a significant difference in the E2F target **(Figure 18A)**. The E2F family transcription factors play significant role in DNA replication, cell proliferation, differentiation, cell cycle regulation, apoptosis. The finding of a significant difference in the E2F target between responders and non-responders in both the desert and excluded immune phenotypes suggests that dysregulation of this pathway could be associated with the response or lack of response to ICI therapy in these phenotypes. The group with high score of E2F pathway was associated with significantly elevated expression of immune checkpoint molecules, including *PD-1* and *PD-L1*⁵⁰. Anti-PD-L1 treatment aims to block the *PD-1* and *PD-L1* interaction, thereby enhancing the anti-tumor immune response. Therefore, a high level of *PD-L1* expression indicates a positive response to anti-*PD-L1* treatment.

In the excluded immune phenotypes, the results of the GSEA of over-exposure genes in respondents compared to nonresponders, confirmed that the *MYC* target and P53 pathway was significantly different **(Figure 18B)**. *MYC* target is included in the cell proliferation-related Hallmark gene sets. the cell proliferation-related pathway scores may have the potential to predict drug treatment response.⁵¹ Recently, *MYC* family members regulate the gene

expression of immune checkpoints, including *PD-1* and *PD-L1*.⁵² As previously stated, a significant amount of *PD-L1* expression can serve as a biomarker for identifying patients who are more likely to respond positively to anti-PD-L1 treatment

The ICI responders in the inflamed immune phenotype reveals an overrepresentation of interleukin 6/Janus kinase/signal transducer and activator of transcription 3 (*IL-6/JAK/STAT3*) signaling (**Figure 18C**). The *IL-6* is regarded as a potential predictive marker for ICI response. Enhance *PD-L1* expression through the *IL-6/JAK/STAT3* signaling pathway in non-small cell lung cancer (NSCLC) cells⁵³. Also, The *IL-6* is associated with poor clinical activity of Atezolizumab (anti-PD-L1) and *IL-6/JAK/STAT3* signaling blocks cytotoxic effector differentiation of CD8+ T cells⁵⁴. Recent studies suggest that Interferon- γ (IFN- γ) is a critical driver of *PD-L1* expression in cancer and host cells.⁵⁵ And IFN- γ -mediated adaptive resistance is one major barrier to improving immunotherapy in solid tumors⁵⁶. *IL-6* can promote T cell exhaustion through *IL-6/STAT3/PD-1* transcription regulation and improve the action of CD4+T cell⁵⁷. The data from this study further substantiate the observation that CD4+ T cell amounts are higher in the response group, with an average of 0.07 compared to an average of 0.04 in the non-response group. (wilcoxon test p-value 0.04)

In the excluded immune phenotype, the TNFA signaling via NF κ B hallmark geneset is significantly enriched in the non-response group compared to the response group. NF- κ B directly induces *PD-L1* gene transcription through promoter binding and can modulate post-transcriptional *PD-L1* expression via indirect pathways⁵⁸. The expression of *PD-L1* in tumor infiltrating macrophages and other myeloid cells is governed by the activity of NF- κ B, a crucial transcription factor⁵⁹. Tumor-associated macrophages (TAMs) are immune cells that infiltrate tumor tissues and are the most abundant immune cells in the tumor microenvironment. A noteworthy association that has been

found is between macrophage infiltration and PD-L1 expression on tumor cells. The macrophage infiltration is highly correlated with increased PD-L1 expression on tumor cells. The dataset from this study shows that the mean value of TAMs is 0.008 in the ICI response group and 0.015 in the non-response group. The difference in TAM levels indicates that the non-response group has a higher prevalence of TAMs than response group (wilcoxon test p-value 0.78).

Aslo, the *KRAS* signaling is enriched in ICI non-response groups in excluded immune phenotype. The activation of *KRAS* on cancer cells extends to the surrounding microenvironment, affecting the properties and functions of its constituents.⁶⁰ The *KRAS* were also described to induce the downregulation of MHC class I molecules and the upregulation of *PD-L1*, reducing the ability of CD8⁺ cytotoxic T cells to recognize and kill cancer cells. Additionally, *KRAS* may drive an anti-inflammatory and pro-tumor immune suppressive microenvironment mediated through *IL-6* secretion. Notably, when *IL-6* was blocked, a reduction of anti-inflammatory macrophage gene expression, and a reduction of the immunosuppressive cytokines *TGF- β* and *IL-10* were observed. Moreover, it has also been described that *IL-6* induces higher levels of T cell exhaustion markers, such as *PD-1*, *CTLA-4*, and *TIM-3*.

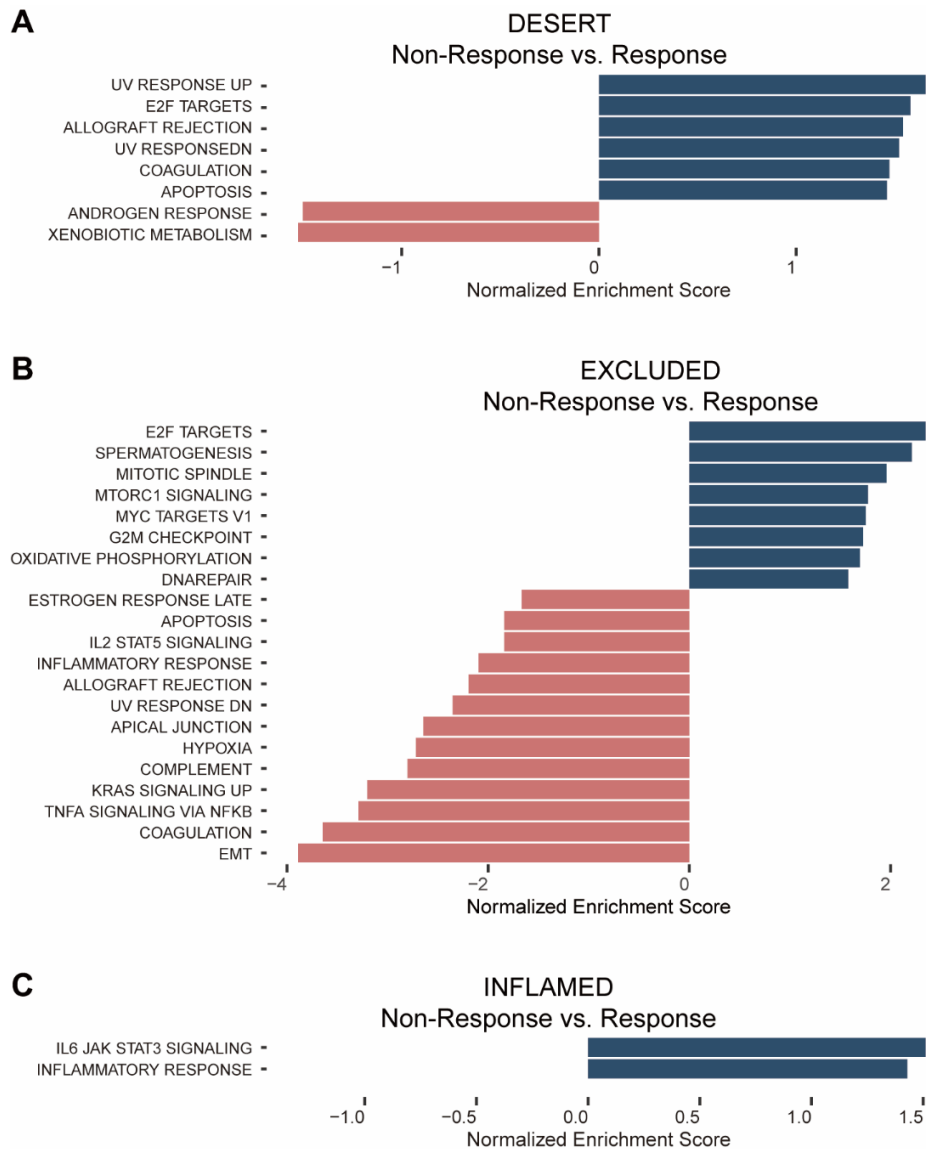


Figure 18. GSEA with hallmark gene-set for immune phenotype-specific ICI response.

(A) Gene Set Enrichment Analysis according to ICI response in desert, (B) excluded, and (C) inflamed immune phenotypes. The blue color labeled the ICI response group, and red labeled the ICI non-response group.

IV. DISCUSSION

In order to perform more efficient patient-specific target immunotherapy, the patient's immune microenvironment should be considered. The immune environment has been determined the prevalence of immune cells based on Immunohistochemistry (IHC), and at the genome level, the immune microenvironment is relatively inferred based on immune signature for a representative of immune populations. The immune phenotype has been associated with significant differences in overall survival among cancer patients receiving ICI treatment. Inflamed immune phenotype may exhibit higher response rates and improved survival outcomes, while excluded and desert immune phenotypes may demonstrate lower response rates and poorer prognosis. Therefore, understanding an individual's immune phenotype is important in predicting their response to ICI therapy and optimizing treatment strategies. In order to increase the effectiveness of personalized immunotherapy for patients, an algorithm for predicting the immune environment at the individual patient based on absolute criteria is required.

Classifying immune phenotypes based on morphology or IHC can be subjective and rely on subjective judgments, leading to reliability and consistency issues. Moreover, the classification criteria may not be clearly defined or compatible with existing diagnostic systems^{19,38,61}. However, using bulk RNA sequencing for immune phenotype classification provides an objective and robust approach. RNA sequencing is an advanced computational technique that analyzes the gene expression profile of immune cells or tissues. It accurately measures the expression levels of hundreds or even thousands of genes, allowing distinction of different immune phenotypes. By analyzing the gene expression profile through bulk RNA sequencing, it becomes possible to objectively classify immune phenotypes based on distinct gene expression patterns. This approach eliminates the subjectivity involved in morphology-based or IHC-based classification and provides a more reliable and standardized method for immune phenotype

characterization. Hence, this study intends to develop an algorithm for predicting immune phenotype-specific ICI response at the individual patient level using gene expression data obtained from bulk RNA sequencing.

The challenges related to the limited number of datasets for immune phenotype classification with bulk RNA sequencing data. These challenges can make it difficult to accurately classify immune phenotypes based on the available datasets. The immune phenotype classification algorithm has been developed with 621 samples collected from 3 different kinds of cancer. The limited sample size prevented the inclusion of melanoma, the primary target of traditional ICI treatments, in the training dataset. Instead, melanoma data from cohort J was used as a validation dataset. The subsequent study aims to develop an algorithm for classifying immunological phenotypes that considers the characteristics of various cancer types, including melanoma. The training and validation datasets used for the construction of the CLIPS prediction model for ICI response have not been used as training datasets in other prediction tools. Furthermore, taking advantage of an independent validation dataset not exposed to any predictive tools enhances the dependability and fairness of the model's performance evaluation. This strategy improves the reliability of the model's ability to make predictions and enables unbiased assessment compared to other ICI response prediction tools. This comprehensive approach rectify the gaps in the previous study and improves the overall understanding of immune phenotypes across different cancer types as well as the accurate prediction ICI response based on the immune phenotypes.

This study revealed that the *PD-1* and *PD-L1* genes, known as biomarkers of the ICI response, may have diversity according to the prevalence of the immune phenotype. Furthermore, if the distribution of immune phenotypes is not different between ICI responders and non-responders, then the expression of the *PD-1* and *PD-L1* genes are likewise consistent at the same level. Therefore, I discovered that *PD-1* and *PD-L1* exhibit associations not only with ICI reactivity but also with immune phenotypes. In previous studies, the presumption that *PD-1* and *PD-L1*

are indicators for ICI response can be inferred from the results that the datasets used in the analysis predominantly consisted of the inflamed immune phenotype. This study presented an important finding about the *PD-1* and *PD-L1* were not only associated with ICI response but also with immune phenotypes. This suggests that *PD-1* and *PD-L1* have a broader influence on immune function beyond their involvement in ICI response. Moreover, the results that identical results were produced in both immune phenotypes defined by IHC and those predicted by CLIPS based on RNA sequencing suggests that immune phenotypes are biologically meaningful.

In this research, I conducted predictions of responsiveness not only for anti-PD-1 monotherapy but also for combination treatment with anti-PD-1 and anti-CTLA-4. From the ERP105482 data resource, the data obtained data from six patients treated with a combination of Nivolumab (anti-PD-1) and Ipilimumab (anti-CTLA-4), as well as data from twenty-five patients treated with a combination of Pembrolizumab (anti-PD-1) and Ipilimumab. A comparative analysis was set up to assess the predictive accuracy of CLIPS–predict IP, CLIPS–no IP, TIDE, and IMPRES with data from thirty-one patients who underwent combination therapies. The accuracy results varied among the different algorithms and treatment regimens. The accuracy of the algorithms for patients treated with Nivolumab and Ipilimumab was as follows: CLIPS–predict IP 0.67, CLIPS–no IP 0.67, TIDE 0.5, and IMPRES 0.67. The accuracy of combination treatment with Pembrolizumab and Ipilimumab data is 0.36 for CLIPS–predict IP, 0.64 for CLIPS–no IP, 0.48 for TIDE, and 0.68 for IMPRES. For the combination treatment data for all 31 samples, the accuracy of CLIPS–predict IP was 0.42, CLIPS–no IP was 0.65, TIDE was 0.48, and IMPRES was 0.68.

The CLIPS–predict IP shows accuracy levels comparable to other predictive tools in the treatment with Nivolumab and Ipilimumab, but it has been found to have lower accuracy in the combination of Pembrolizumab and Ipilimumab. The accuracy seems to be somewhat lacking because DEGs that did not consider the

reactivity to combination treatment were used for model construction. The use of DEGs that did not consider responsiveness to combination treatment in model construction appears to have led to a minor decrease in accuracy. While the IMPRES model might seem to have a high level of accuracy, an in-depth examination of **Table 6** reveals that all predictions are classified as belonging to the response group. The performance of CLIPS–no IP shows high efficacy in combination treatment with Pembrolizumab and Ipilimumab, second only to IMPRES. This suggests that CLIPS–no IP may be a suitable tool for predicting the effectiveness of combination treatments. However, it is important to note that CLIPS–no IP, like IMPRES, has a bias in predictions when applied to combination treatment with Nivolumab and Ipilimumab. In the case of TIDE, the lowest performance compared to other predictions within combination treatment. TIDE has been observed to tend to generate non-response predictions, similar to the previous findings. This means that the predictions produced by TIDE are less likely to dynamically adjust to changes in the input data. This bias undermines the reliability and generalizability of the model's predictions, indicating a need for further refinement. The upcoming study aims to incorporate the combination treatment dataset into the training dataset to improve the accuracy of predicting ICI responsiveness in preparation for various ICI therapy scenarios.

There may be doubts about whether classifying immune phenotypes into two distinct cases that sharply differ would lead to better discernment. However, this study confirmed significant differences in gene expression within the excluded immune phenotype and the desert and inflamed immune phenotypes. And by incorporating these differences in immune phenotypes, I have developed a more improved ICI response prediction model. As an advantage of detailed classification, the classification of immune phenotypes can enhance the application of alternative therapies for patients who fail to show a response to ICI. The immune phenotypes excluded and desert do not react to anti-PD-1 therapy and are classified as cold tumors. The excluded and desert phenotypes do not respond

to anti-PD1 and can be considered variants of cold tumors. In the case of the excluded phenotype, it is asserted that FDA-approved inhibitors of TGF- β , such as inhibitors of VEGF receptor kinases, have been used for the treatment for hepatocellular carcinoma⁶². Also, understanding the NF- κ B-mediated expression of *PD-L1* and its relationship with tumor-associated macrophages (TAMs) can provide valuable insights into the intricate interplay between tumor cells, immune cells, and the TME. NF- κ B can directly regulate *PD-L1* expression in macrophages and other myeloid cells when stimulated by inflammatory cytokines. Numerous studies have revealed the significance of NF- κ B activation and TAMs abundance in modulating the response to ICI. Previous research suggests that the combined administration of NF- κ B inhibitors with ICI represents a promising new approach to cancer treatment⁶³.

In case the inflamed phenotype of ICI nonresponder, treating this phenotype with a combination of several ICI or priming with CSF1R inhibitors might prove to be beneficial. The combination of CSF1R inhibitors and ICI has been shown to boost the effectiveness of ICI, specifically in treating colorectal cancer⁶⁴. IL-6 activates CD4+ T cells and interacts with TGF- β to induce differentiation into regulatory T cell (T reg), thereby evading immune responses. Upon reviewing our data, we observed that CD4+ T cells were statistically significantly higher in the response group, while an average amount of T reg is not statistically significant difference. (R 0.0137 vs NR 0.014, wilcoxon test p-value 0.99). This indicates that the response group consists of a substantial number of CD4+T cells that can initiate immunological reactions. So, the response group would have been more effective than treating with anti-PD-1. Exhausted T cells in inflamed immune phenotype are statistically significantly higher than other immune phenotypes (kruskal test p-value 0.99). For patients who do not respond to treatment and have inflammation, combining anti-PD-1 and IL-6 blocking is presumed to be a more effective approach.

In conclusion, this study will emphasize the importance of immune phenotype in

ICI responsiveness prediction and expand the research to help predict the treatment of patients. This observation implies that applying CLIPS may be beneficial in guiding the following design of studies related to immunotherapy and contribute to the overall advancement of cancer treatment.

Table 6. Confusion matrix of independent validation with combination treatment

Type of combination treatment	Method	Predicted ICI response	Actual Response (CR + PR)	Actual Non-Response (SD +PD)
anti-PD-1 + anti-CTLA-4 (Nivolumab + Ipilimumab)	CLIPS – predict IP	Response	3	1
		Non-Response	1	1
	CLIPS – no IP	Response	4	2
		Non-Response	0	0
anti-PD-1 + anti-CTLA-4 (Pembrolizumab + Ipilimumab)	TIDE	Response	1	0
		Non-Response	3	2
	IMPRES	Response	4	2
		Non-Response	0	0
anti-PD-1 + anti-CTLA-4 (Pembrolizumab + Ipilimumab)	CLIPS – predict IP	Response	6	6
		Non-Response	10	3
	CLIPS – no IP	Response	11	4
		Non-Response	5	3
anti-PD-1 + anti-CTLA-4 (Pembrolizumab + Ipilimumab)	TIDE	Response	4	1
		Non-Response	12	8
	IMPRES	Response	16	8
		Non-Response	0	1

V. CONCLUSION

The immune phenotype is an important factor affecting ICI responsiveness. It refers to the unique characteristics of an individual's immune system, including the composition and activity of immune cells, expression of immune-related genes, and interactions within the tumor microenvironment. The immune phenotype is associated with significant differences in overall survival. The inflamed immune phenotype improves survival outcomes compared to excluded and desert immune phenotypes.

To improve the effectiveness of personalized immunotherapy, it is essential to develop an algorithm that can accurately predict ICI response based on immune phenotype. The study revealed that accurately predicting the response to immune checkpoint inhibitors (ICI) was more feasible by first identifying the immune phenotype of the patient, as opposed to simply predicting ICI responses. In this study, I have developed an immune phenotype prediction model that can potentially replace Immunohistochemistry (IHC). The CLIPS (Classification of Immune Phenotypes-Specific ICI response) can predict immune phenotype from bulk RNA sequencing data with an accuracy of 0.76. The CLIPS provides three distinct operating modes for predicting ICI response based on specific immunological phenotypes. Each mode utilizes a unique approach to handle immune phenotypic information. According to the evaluation results on the test dataset, CLIPS-known IP and CLIPS-predict IP demonstrate superior performance compared to conventional methods such as TIDE and IMPRES. Within the independent melanoma test set, CLIPS-predict IP demonstrates more accurate results with 0.76 accuracy compared to alternative predictive tools (TIDE 0.63 vs IMPRES 0.58). Furthermore, CLIPS exhibited superior predictive performance across all cancer types, outperforming other ICI response prediction methods, in a comparative study involving melanoma, lung cancer, and gastric cancer. Also, To determine whether there is bias in predictions based on different types of ICI treatments, the responsiveness of Nivolumab and Pembrolizumab was

predicted. CLIPS demonstrated outstanding performance and provided well-balanced forecasts in both cases.

This study presented the significant differences in *PD-1* and *PD-L1* expressions based on immune phenotype, even though there was no difference in gene expression depending on ICI response. These findings provide insight into the complex connection between immune phenotype and the absence of *PD-1* and *PD-L1*, emphasizing the potential influence on the effectiveness of ICI.

To provide further insight, I analyzed genomic characteristics associated with ICI response based on immune phenotype. Notably, the E2F pathways enriched in the ICI response group in the excluded and desert immune phenotypes. The E2F pathway appears to enhance *PD-1* gene expression, increasing susceptibility to anti-PD1 treatments. In the inflamed immune phenotype, ICI response groups demonstrated a notable overrepresentation of the IL-6/JAK/STAT3 signaling pathway. IL-6 has been identified as a potential predictor of ICI responses due to its ability to increase the expression of *PD-1*. In the non-response group within the excluded immune phenotype, there is a notable enrichment of the TNFA signaling via NFκB hallmark geneset compared to the response group. The NF-κB activity plays an important role in modulating the expression of *PD-L1* in tumor infiltrating macrophages and other myeloid cells. These findings highlight the importance of NF-κB as a key regulator in modulating the immune response.

The notable advantage of CLIPS, which distinguishes it from existing methods, is that it is a more advanced model that can further refine and predict reactivity due to differences in reactivity by immune phenotype. In this study, we endeavored to innovate a novel approach towards the classification of immune phenotypes, circumventing the traditional reliance on IHC. By employing alternative methodological approaches, our objective was to expand our comprehension of the characteristics and functions of immune phenotypes. The findings suggest that partitioning ICI response across immune phenotypes yields superior results compared to predictions solely based on primary ICI reactivity data.

In conclusion, the immune phenotype acts as a filter in one of the processes of predicting ICI response, enabling more balanced and accurated predictions. This study highlights the significance of immune phenotypes in predicting ICI responsiveness and guiding personalized treatment strategies.

REFERENCES

1. Oiseth SJ, Aziz MS. Cancer immunotherapy: a brief review of the history, possibilities, and challenges ahead. *Journal of Cancer Metastasis and Treatment* 2017;3.
2. Xie N, Shen G, Gao W, Huang Z, Huang C, Fu L. Neoantigens: promising targets for cancer therapy. *Signal Transduct Target Ther* 2023;8:9.
3. Morrison C, Pabla S, Conroy JM, Nesline MK, Glenn ST, Dressman D, et al. Predicting response to checkpoint inhibitors in melanoma beyond PD-L1 and mutational burden. *J Immunother Cancer* 2018;6:32.
4. Thorsson V, Gibbs DL, Brown SD, Wolf D, Bortone DS, Ou Yang TH, et al. The Immune Landscape of Cancer. *Immunity* 2019;51:411-2.
5. Le DT, Uram JN, Wang H, Bartlett BR, Kemberling H, Eyring AD, et al. PD-1 Blockade in Tumors with Mismatch-Repair Deficiency. *N Engl J Med* 2015;372:2509-20.
6. Cogdill AP, Andrews MC, Wargo JA. Hallmarks of response to immune checkpoint blockade. *Br J Cancer* 2017;117:1-7.
7. Bohaumilitzky L, von Knebel Doeberitz M, Kloor M, Ahadova A. Implications of Hereditary Origin on the Immune Phenotype of Mismatch Repair-Deficient Cancers: Systematic Literature Review. *J Clin Med* 2020;9.
8. Tumeh PC, Harview CL, Yearley JH, Shintaku IP, Taylor EJ, Robert L, et al. PD-1 blockade induces responses by inhibiting adaptive immune resistance. *Nature* 2014;515:568-71.
9. Mariathasan S, Turley SJ, Nickles D, Castiglioni A, Yuen K, Wang Y, et al. TGFbeta attenuates tumour response to PD-L1 blockade by contributing to exclusion of T cells. *Nature* 2018;554:544-8.
10. Junttila MR, de Sauvage FJ. Influence of tumour micro-environment heterogeneity on therapeutic response. *Nature* 2013;501:346-54.
11. Binnewies M, Roberts EW, Kersten K, Chan V, Fearon DF, Merad M, et al. Understanding the tumor immune microenvironment (TIME) for effective

- therapy. *Nat Med* 2018;24:541-50.
12. Tiwari A, Oravec T, Dillon LA, Italiano A, Audoly L, Fridman WH, et al. Towards a consensus definition of immune exclusion in cancer. *Front Immunol* 2023;14:1084887.
 13. Phillips D, Matusiak M, Gutierrez BR, Bhate SS, Barlow GL, Jiang S, et al. Immune cell topography predicts response to PD-1 blockade in cutaneous T cell lymphoma. *Nat Commun* 2021;12:6726.
 14. Wang L, Geng H, Liu Y, Liu L, Chen Y, Wu F, et al. Hot and cold tumors: Immunological features and the therapeutic strategies. *MedComm* (2020) 2023;4:e343.
 15. Chen DS, Mellman I. Elements of cancer immunity and the cancer-immune set point. *Nature* 2017;541:321-30.
 16. Duan J, Wang Y, Jiao S. Checkpoint blockade-based immunotherapy in the context of tumor microenvironment: Opportunities and challenges. *Cancer Med* 2018;7:4517-29.
 17. Liu YT, Sun ZJ. Turning cold tumors into hot tumors by improving T-cell infiltration. *Theranostics* 2021;11:5365-86.
 18. Yi M, Jiao D, Xu H, Liu Q, Zhao W, Han X, et al. Biomarkers for predicting efficacy of PD-1/PD-L1 inhibitors. *Mol Cancer* 2018;17:129.
 19. Chakiryan NH, Kim Y, Berglund A, Chang A, Kimmel GJ, Hajiran A, et al. Geospatial characterization of immune cell distributions and dynamics across the microenvironment in clear cell renal cell carcinoma. *J Immunother Cancer* 2023;11.
 20. Desbois M, Udyavar AR, Ryner L, Kozlowski C, Guan Y, Durrbaum M, et al. Integrated digital pathology and transcriptome analysis identifies molecular mediators of T-cell exclusion in ovarian cancer. *Nat Commun* 2020;11:5583.
 21. Hornburg M, Desbois M, Lu S, Guan Y, Lo AA, Kaufman S, et al. Single-cell dissection of cellular components and interactions shaping the tumor immune phenotypes in ovarian cancer. *Cancer Cell* 2021;39:928-44 e6.

22. Plaschka M, Benboubker V, Grimont M, Berthet J, Tonon L, Lopez J, et al. ZEB1 transcription factor promotes immune escape in melanoma. *J Immunother Cancer* 2022;10.
23. Kim JH, Seo M-K, Lee JA, Yoo S-Y, Oh HJ, Kang H, et al. Genomic and transcriptomic characterization of heterogeneous immune subgroups of microsatellite instability-high colorectal cancers. *Journal for ImmunoTherapy of Cancer* 2021;9.
24. Gide TN, Quek C, Menzies AM, Tasker AT, Shang P, Holst J, et al. Distinct Immune Cell Populations Define Response to Anti-PD-1 Monotherapy and Anti-PD-1/Anti-CTLA-4 Combined Therapy. *Cancer Cell* 2019;35:238-55 e6.
25. Kim ST, Cristescu R, Bass AJ, Kim KM, Odegaard JI, Kim K, et al. Comprehensive molecular characterization of clinical responses to PD-1 inhibition in metastatic gastric cancer. *Nat Med* 2018;24:1449-58.
26. Cho JW, Hong MH, Ha SJ, Kim YJ, Cho BC, Lee I, et al. Genome-wide identification of differentially methylated promoters and enhancers associated with response to anti-PD-1 therapy in non-small cell lung cancer. *Exp Mol Med* 2020;52:1550-63.
27. Jung H, Kim HS, Kim JY, Sun JM, Ahn JS, Ahn MJ, et al. DNA methylation loss promotes immune evasion of tumours with high mutation and copy number load. *Nat Commun* 2019;10:4278.
28. Dobin A, Davis CA, Schlesinger F, Drenkow J, Zaleski C, Jha S, et al. STAR: ultrafast universal RNA-seq aligner. *Bioinformatics* 2012;29:15-21.
29. Li B, Dewey CN. RSEM: accurate transcript quantification from RNA-Seq data with or without a reference genome. *BMC Bioinformatics* 2011;12:323.
30. Smid M, Coebergh van den Braak RRJ, van de Werken HJG, van Riet J, van Galen A, de Weerd V, et al. Gene length corrected trimmed mean of M-values (GeTMM) processing of RNA-seq data performs similarly in intersample analyses while improving intrasample comparisons. *BMC Bioinformatics* 2018;19:236.

31. Robinson MD, McCarthy DJ, Smyth GK. edgeR: a Bioconductor package for differential expression analysis of digital gene expression data. *Bioinformatics* 2010;26:139-40.
32. Risso D, Ngai J, Speed TP, Dudoit S. Normalization of RNA-seq data using factor analysis of control genes or samples. *Nat Biotechnol* 2014;32:896-902.
33. Zhang Y, Parmigiani G, Johnson WE. ComBat-seq: batch effect adjustment for RNA-seq count data. *NAR Genom Bioinform* 2020;2:lqaa078.
34. Love MI, Huber W, Anders S. Moderated estimation of fold change and dispersion for RNA-seq data with DESeq2. *Genome Biol* 2014;15:550.
35. Sturm G, Finotello F, List M. Immunedeconv: An R Package for Unified Access to Computational Methods for Estimating Immune Cell Fractions from Bulk RNA-Sequencing Data. In: Boegel S, editor. *Bioinformatics for Cancer Immunotherapy: Methods and Protocols*. New York, NY: Springer US; 2020. p.223-32.
36. Racle J, Gfeller D. EPIC: A Tool to Estimate the Proportions of Different Cell Types from Bulk Gene Expression Data. In: Boegel S, editor. *Bioinformatics for Cancer Immunotherapy: Methods and Protocols*. New York, NY: Springer US; 2020. p.233-48.
37. Yoshihara K, Shahmoradgoli M, Martinez E, Vegesna R, Kim H, Torres-Garcia W, et al. Inferring tumour purity and stromal and immune cell admixture from expression data. *Nat Commun* 2013;4:2612.
38. Hammerl D, Martens JWM, Timmermans M, Smid M, Trapman-Jansen AM, Foekens R, et al. Spatial immunophenotypes predict response to anti-PD1 treatment and capture distinct paths of T cell evasion in triple negative breast cancer. *Nat Commun* 2021;12:5668.
39. Danaher P, Warren S, Lu R, Samayoa J, Sullivan A, Pekker I, et al. Pan-cancer adaptive immune resistance as defined by the Tumor Inflammation Signature (TIS): results from The Cancer Genome Atlas (TCGA). *J Immunother Cancer* 2018;6:63.

40. Charoentong P, Finotello F, Angelova M, Mayer C, Efremova M, Rieder D, et al. Pan-cancer Immunogenomic Analyses Reveal Genotype-Immunophenotype Relationships and Predictors of Response to Checkpoint Blockade. *Cell Rep* 2017;18:248-62.
41. Rooney MS, Shukla SA, Wu CJ, Getz G, Hacohen N. Molecular and genetic properties of tumors associated with local immune cytolytic activity. *Cell* 2015;160:48-61.
42. Jiang P, Gu S, Pan D, Fu J, Sahu A, Hu X, et al. Signatures of T cell dysfunction and exclusion predict cancer immunotherapy response. *Nat Med* 2018;24:1550-8.
43. Auslander N, Zhang G, Lee JS, Frederick DT, Miao B, Moll T, et al. Robust prediction of response to immune checkpoint blockade therapy in metastatic melanoma. *Nat Med* 2018;24:1545-9.
44. Liberzon A, Birger C, Thorvaldsdottir H, Ghandi M, Mesirov JP, Tamayo P. The Molecular Signatures Database (MSigDB) hallmark gene set collection. *Cell Syst* 2015;1:417-25.
45. Korotkevich G, Sukhov V, Budin N, Shpak B, Artyomov MN, Sergushichev A. 2021.
46. Tang Q, Chen Y, Li X, Long S, Shi Y, Yu Y, et al. The role of PD-1/PD-L1 and application of immune-checkpoint inhibitors in human cancers. *Frontiers in Immunology* 2022;13.
47. Bai R, Lv Z, Xu D, Cui J. Predictive biomarkers for cancer immunotherapy with immune checkpoint inhibitors. *Biomark Res* 2020;8:34.
48. Chatziioannou E, Leiter U, Thomas I, Keim U, Seeber O, Meiwes A, et al. Features and Long-Term Outcomes of Stage IV Melanoma Patients Achieving Complete Response Under Anti-PD-1-Based Immunotherapy. *Am J Clin Dermatol* 2023;24:453-67.
49. Chicco D, Jurman G. The advantages of the Matthews correlation coefficient (MCC) over F1 score and accuracy in binary classification evaluation. *BMC*

- Genomics 2020;21:6.
50. Oshi M, Takahashi H, Tokumaru Y, Yan L, Rashid OM, Nagahashi M, et al. The E2F Pathway Score as a Predictive Biomarker of Response to Neoadjuvant Therapy in ER+/HER2- Breast Cancer. *Cells*; 2020.
 51. Oshi M, Patel A, Le L, Tokumaru Y, Yan L, Matsuyama R, et al. G2M checkpoint pathway alone is associated with drug response and survival among cell proliferation-related pathways in pancreatic cancer. *Am J Cancer Res* 2021;11:3070-84.
 52. Casey SC, Baylot V, Felsher DW. The MYC oncogene is a global regulator of the immune response. *Blood* 2018;131:2007-15.
 53. Zhang N, Zeng Y, Du W, Zhu J, Shen D, Liu Z, et al. The EGFR pathway is involved in the regulation of PD-L1 expression via the IL-6/JAK/STAT3 signaling pathway in EGFR-mutated non-small cell lung cancer. *Int J Oncol* 2016;49:1360-8.
 54. Huseni MA, Wang L, Klementowicz JE, Yuen K, Breart B, Orr C, et al. CD8(+) T cell-intrinsic IL-6 signaling promotes resistance to anti-PD-L1 immunotherapy. *Cell Rep Med* 2023;4:100878.
 55. Abiko K, Matsumura N, Hamanishi J, Horikawa N, Murakami R, Yamaguchi K, et al. IFN-gamma from lymphocytes induces PD-L1 expression and promotes progression of ovarian cancer. *Br J Cancer* 2015;112:1501-9.
 56. Yu M, Peng Z, Qin M, Liu Y, Wang J, Zhang C, et al. Interferon- γ induces tumor resistance to anti-PD-1 immunotherapy by promoting YAP phase separation. *Mol Cell* 2021;81:1216-30.e9.
 57. Fang L, Liu K, Liu C, Wang X, Ma W, Xu W, et al. Tumor accomplice: T cell exhaustion induced by chronic inflammation. *Front Immunol* 2022;13:979116.
 58. Antonangeli F, Natalini A, Garassino MC, Sica A, Santoni A, Di Rosa F. Regulation of PD-L1 Expression by NF-kappaB in Cancer. *Front Immunol* 2020;11:584626.
 59. Ju X, Zhang H, Zhou Z, Chen M, Wang Q. Tumor-associated macrophages

- induce PD-L1 expression in gastric cancer cells through IL-6 and TNF- α signaling. *Exp Cell Res* 2020;396:112315.
60. Dias Carvalho P, Guimaraes CF, Cardoso AP, Mendonca S, Costa AM, Oliveira MJ, et al. KRAS Oncogenic Signaling Extends beyond Cancer Cells to Orchestrate the Microenvironment. *Cancer Res* 2018;78:7-14.
 61. Kather JN, Suarez-Carmona M, Charoentong P, Weis CA, Hirsch D, Bankhead P, et al. Topography of cancer-associated immune cells in human solid tumors. *Elife* 2018;7.
 62. Finn RS, Qin S, Ikeda M, Galle PR, Ducreux M, Kim TY, et al. Atezolizumab plus Bevacizumab in Unresectable Hepatocellular Carcinoma. *N Engl J Med* 2020;382:1894-905.
 63. Betzler AC, Theodoraki MN, Schuler PJ, Doscher J, Laban S, Hoffmann TK, et al. NF-kappaB and Its Role in Checkpoint Control. *Int J Mol Sci* 2020;21.
 64. Cannarile MA, Weisser M, Jacob W, Jegg AM, Ries CH, Ruttinger D. Colony-stimulating factor 1 receptor (CSF1R) inhibitors in cancer therapy. *J Immunother Cancer* 2017;5:53.

APPENDICES

CLIPS – Classification of Immune Phenotypes-Specific ICI response

CR – Complete response

CTLA-4 – Cytotoxic T-lymphocyte-associated protein 4

DEG – Differential gene expression

GeTMM – Gene length corrected trimmed mean of M-values

GSEA – Gene Set Enrichment Analysis

ICI – Immune checkpoint inhibitor

IDO – Indoleamine 2,3-dioxygenase

IHC – Immunohistochemistry

IMPRES – IMMuno-PREdictive Score

LAG-3 – Lymphocyte-activation gene 3

NR – Nonresponder for ICI treatment

PD – Progressive disease

PD-1 – Programmed cell death protein 1

PD-L1 – Programmed death-ligand 1

PR – Partial response

R – Responder for ICI treatment

SD – Stable disease

TIDE – Tumor Immune Dysfunction and Exclusion

TILs – Tumor-infiltrating lymphocytes

TME – Tumor microenvironment

ABSTRACT(IN KOREAN)

면역 표현형 분류 기반 면역관문억제제 반응성 예측

<지도교수 김상우>

연세대학교 대학원 의과학과

김은영

면역 표현형은 암에 대한 면역력을 반영하며 면역 반응이 암을 제거하는 것을 방해할 수 있는 생물학적 메커니즘과 관련이 있다. 또한 면역 표현형은 면역관문억제제 치료를 받은 흑색종 환자의 전체 생존율에도 영향을 미친다. 이러한 이유로 환자 맞춤형 면역 치료의 효과를 높이기 위해서는 환자 개인의 면역 환경을 객관적으로 정확하게 예측할 수 있는 알고리즘 개발이 필수적이다. 본 연구의 목적은 bulk RNA 시퀀싱 데이터의 유전자 발현 데이터를 활용하여 환자 개인의 면역 표현형을 예측하고, 이를 바탕으로 ICI response를 예측할 수 있는 알고리즘을 구축하는 것이다. 연구에서 개발한 CLIPS (Classification of Immune Phenotypes-Specific ICI response)는 면역 표현형 특이적 면역관문억제제 반응 예측 알고리즘이다. CLIPS는 bulk RNA 시퀀싱 데이터로부터 0.76의 ACU의 성능을 가지고 환자 특이적인 면역 표현형을 강건한 예측할

수 있어, 기존의 면역조직화학 기법을 대체할 수 있다.

예측 모델의 검증을 위해서, 흑색종 환자 41명의 독립적인 검증 데이터 기준으로 기존에 알려진 2개의 면역관문억제제 반응성 예측 도구인 TIDE와 IMPRES의 정확도를 CLIPS와 비교하였다. 그 결과, TIDE는 0.63, IMPRES는 0.58의 정확도를 가지고 있다. CLIPS는 면역 표현형을 예측 분류하고, 이를 기반으로 개별 환자의 면역관문억제제 반응을 제시하여 정확도 0.76으로 보다 더 정확한 예측이 가능하다. CLIPS는 암 종 또는 ICI 약물 종류에 구분없이 높은 정확도를 가지고 반응성 예측이 가능하다.

나아가 본 연구에서는 *PD-1* 와 *PD-L1*의 발현이 면역관문억제제 반응성에 대한 지표뿐만 아니라, 면역 표현형과 연관성이 있음을 밝혔다. *PD-1* 와 *PD-L1* 유전자의 발현은 excluded와 desert 면역 표현형 대비, inflamed 면역 표현형에서 통계적으로 유의하게 높은 값으로 존재하고 있다. 또한 excluded 면역 표현형과 desert 면역 표현형의 면역관문억제제 반응 그룹에서 공통으로 Hallmark 유전자 세트 중, E2F 경로와 관련된 발현이 증가한 것을 확인하였다. E2F 경로는 *PD-1* 유전자 발현을 증가시켜서 면역 관문억제제에 대한 감수성을 증가시키는 것으로 보인다. 그리고 IL-6/JAK/STAT3 신호 전달은 inflamed 면역 표현형의 면역관문억제제 반응 그룹에서 우세하게 존재한다. 이는 IL-6 분비를 통해 *PD-L1*의 유전자 발현을 증가시켰기에 면역 관문억제제에 좋은 반응성을 기대할 수 있다.

본 연구는 면역 표현형을 구분하는 명확한 전략을 수립함으로써 개인에 맞춤형 치료법을 개발하는 데 중요한 참고 자료가 될 것이다.

면역 표현형은 면역 체계의 기능적 특징을 이해하는 데 도움을 주며, 면역관문억제제 반응을 예측하는 데 사용될 수 있는 추가적인 하위 유형을 확장한다.

결론적으로, 본 연구는 면역 표현형의 이해와 예측을 통해 개인에게 맞춤형 치료법을 제공하는 것에 큰 기여를 할 것이다. 이를 통해 암 환자들의 생존율을 향상시키고 면역 치료의 효과를 극대화할 수 있을 것으로 기대된다.

핵심되는 말 : 면역 표현형, 면역 관문억제제, 면역 프로파일링, 면역 요법, 종양 미세환경, 면역 정보학, 차세대 시퀀싱

PUBLICATION LIST

1. Kim S, Kim HS, **Kim E**, Lee MG, Shin EC, Paik S, et al. Neopepsee: accurate genome-level prediction of neoantigens by harnessing sequence and amino acid immunogenicity information. *Ann Oncol* 2018;29:1030-6.
2. Jo SY, **Kim E**, Kim S. Impact of mouse contamination in genomic profiling of patient-derived models and best practice for robust analysis. *Genome Biol* 2019;20:231.
3. Lee HS, **Kim E**, Lee J, Park SJ, Hwang HK, Park CH, et al. Profiling of conditionally reprogrammed cell lines for in vitro chemotherapy response prediction of pancreatic cancer. *EBioMedicine* 2021;65:103218.
4. Lim SM, **Kim E**, Jung KH, Kim S, Koo JS, Kim SI, et al. Genomic landscape of extraordinary responses in metastatic breast cancer. *Commun Biol* 2021;4:449.
5. Yang Y, **Kim E**, Kim S. Insignificant effects of loss of heterozygosity in HLA in the efficacy of immune checkpoint blockade treatment. *Genes Genomics* 2022;44:509-15.